Single Molecule Study of RNA Polymerase Transcription Under Load

Keir Cajal Neuman

A DISSERTATION

PRESENTED TO THE FACULTY

OF PRINCETON UNIVERSITY

IN CANDIDACY FOR THE DEGREE

OF DOCTOR OF PHILOSPHY

RECOMMENDED FOR ACCEPTANCE

BY THE DEPARTMENT OF PHYSICS

November 2002

Abstract

RNA Polymerase (RNAP) is responsible for transcribing genes encoded in DNA into an RNA message that is subsequently translated into a polypeptide chain, which folds to become a functional protein. Due to its unique position in the flow of genetic information from gene to protein, RNAP is a primary point of regulation of gene expression and consequently is of crucial importance. In this dissertation we present single-molecule optical trapping measurements of *Escherichia coli (E. coli)* RNAP transcribing under load. In addition we present several technical improvements in optical trapping that were developed in preparation for the study on RNAP.

Optical trapping methods have been touted as a non-invasive means to manipulate biological specimens. This is only partially true, as the intense focus of the trapping laser will eventually destroy the trapped specimen in a process that has been termed "opticution." We determined the wavelength dependence of photodamage to *E. coli* over the near infrared region of the spectrum. Additionally, we showed that photodamage can be prevented by removing the molecular oxygen from the trapping medium.

Optical traps have traditionally been employed to produce force and measure displacement in the lateral plane. We present a method of measuring both relative and absolute axial displacements of trapped particles and we use this ability to make novel measurements of optical trapping forces.

RNA polymerase (RNAP) translocates along a DNA template with variable rates and frequent pauses. To investigate the mechanisms of transcription, we have determined the effect of hindering and assisting forces on the transcriptional velocity and pausing of single *E. coli* RNAP molecules, using an optical trap that allows the detection of pauses as short as one second. Although our naturally transcribed template lacks known regulatory pauses, we detected a class of short pauses that are not the result of RNAP backtracking along the template. Additionally, we observe a population velocity distribution that implies multiple velocity states, although individual molecules appear to move with a single velocity.

For Adah

Acknowledgments

Over the course of a long and enjoyable graduate career I have been fortunate to receive help, guidance and support from many people. It is a unique pleasure to acknowledge the contributions these people have made to this thesis, which owes its existence to their efforts.

Primary among these people is my advisor, Steven Block. Steve's enthusiasm and passion for science are inspiring and contagious. During my time in his lab Steve has given me the freedom and the support to explore while providing the subtle guidance that kept me from getting lost. Steve has also taught me the crucial importance of presenting my thoughts and my work clearly and precisely. He has suffered through my poorly spelled and incoherent, stream-of-conscience presentations and manuscripts, never tiring of providing advice and suggestions. Most importantly, Steve has created a rich, vibrant environment for learning and pursuing ideas.

Integral to this environment are the students, post-docs and staff who make their unique contributions. At Princeton, I was in awe of the group I joined. Mark Schnitzer was, and continues to be, encouraging and inspiring. He went a long way in making me feel like I belonged in the lab. Lisa Satterwhite bore the brunt of my initial ignorance of biology. She was patient and encouraging, answering all of my questions and providing not just the answers but also the correct approach to the problems I had. Koen Visscher taught

me about optical trapping and optics. Never condescending, always fun, and usually over a cup of coffee, he would share is immense wealth of knowledge with me. He continues to be a source of advice and inspiration. Michelle Wang introduced me to RNA polymerase and has been supportive and encouraging while I continued the project she started. Steve Gross broadened my scientific horizons through his creative approach to problems and wide interests. Tom Perkins has provided an example and eased my entry into the world of nucleic-acid enzymes. Matt Lang will be breathing easier now that I have finally written my thesis. He, more than anyone, has looked out for my well being and has constantly prodded me along. I would not have survived the move to Stanford without him.

At Stanford, I have been fortunate to work with another group of talented and fun individuals. Elio Abbondanzieri has worked with me since joining the lab. The majority of the work in this thesis was accomplished with his help; his keen insight and intelligence have been invaluable. Chip Asbury has patiently thought through many aspects of this work with me, never satisfied until I can explain every detail. He has helped bring clarity and focus, and he introduced me to "west-coast" mountain biking. Josh Shaevitz is always ready and willing to argue about an idea or a problem, preferably over a beer. Ravi Dalal kept me company many long nights in the lab and has been the DJ since he joined the group. Polly Fordyce has brought a great deal of fun and spunk to the lab in addition to raising our ecological awareness. Adrian Fehr introduced the lab to the wide world of fine tea. Kristina Herbert is the newest member of the lab and I am

excited that she will be bringing her knowledge and skills to bear on the continuation of the RNAP project.

I have been fortunate to be involved in collaborations with different labs. Jeff Gelles and Bob Landick have been practically co-advisors for the RNA polymerase work. Our monthly teleconferences kept me on track and their combined insight and knowledge helped make sense of and give direction to the data I collected. I am also indebted to Oi Kwan Wong in Jeff's lab for help with the RNA polymerase assay. Anita Engh, also from Jeff's lab, first taught me the polymerase assay when she was an undergraduate. As a graduate student at Stanford she was instrumental in organizing an RNAP journal club and has been generous with her time and energy. At Princeton, Keren Bergman first took me on to work on the photo-damage project and allowed me to dabble in other aspects of her lab. Her constant encouragement gave me the confidence to take on my first completely independent research project, which set me on the path to eventually writing this thesis.

One of the pleasures of being a grad student is the opportunity to work with, supervise and mentor undergraduate students. Several students worked with me at Princeton on the photodamage project. Grace Liou helped me build the tunable optical trap and perfect the damage assay. She was also instrumental in keeping the project alive and progressing during my hiatus from the lab. Anja Brau assisted with the work on anaerobic trapping conditions. Ed Chadd, known to the lab as "Ed the machine," helped me wrap up the damage project and left an indelible mark on the Princeton Biology department with his

"interpretive dance of the *E. coli*". At Stanford the undergraduates have been equally as impressive. Mithun Patel and Sridhar Dronavalli took on a project that had been considered too difficult by our collaborators, and proceeded to develop a series of novel techniques to address the problem. Becky Wong has recently joined team RNAP and is making progress on her project, while keeping the grad students in line. Part of my interest in working with undergraduates is as a form of repayment to the graduate student, Tom Donnelly, who took me under his wing when I was an undergrad in his lab. He, more than anyone, taught me what it means to do research and to work in a lab. Only by trying to follow his example can I possibly thank him for all he has done.

In addition to the scientific help and guidance I have received, several people have gone out of their way to make life easier and more pleasant. Laurel Lerner at Princeton has been amazingly patient with my scattered academic career and has helped me in countless ways throughout it. She will be pleased to put my very thick file into the "graduated" file drawer. Carol Killian at Stanford has adopted the entire lab and assigned herself as "Lab Mom". Steve's administrative assistants have added to the atmosphere in the lab. Susan Lacoste's impossibly quirky sense of humor and impeccable fashion sense will live on in Block lab history. Jolande Murray has brought wit, flair, and some very good deserts to the Block lab. She is much more that we possibly deserve.

Several people at Princeton helped in making my time there fun and memorable. Rudro, Rich, Kasia, Majid, Rikki and Malcolm were friends through it all. Mara introduced me to cycling and explored a good portion of the NJ trails with me.

My family has supported me throughout my educational pursuits, offering advice with tough decisions and encouraging me when I was frustrated. Additionally, my father has given me technical advice on numerous occasions and has read and edited all of my manuscripts. This dissertation owes a great deal to his patient editing of multiple drafts.

I have a second family to thank for their support and friendship. Dr and Mrs. Liou and Gary and Joyce have treated me like a family member for the past several years. I am indebted to them for their kindness and generosity to my family and me.

Finally I would like to thank three people, without whom this thesis may not have been written.

Christos and Eva. Without you I don't think I would have made it.

Grace. Thank you. This dissertation is a testament to your love and support.

Contents

Introduction

RNA polymerase (RNAP) plays a pivotal role in the flow of genetic information from DNA to the synthesis of proteins encoded by the DNA. It is responsible for transcribing the DNA sequence into an RNA intermediate, which directs the synthesis of proteins through the translation of the RNA message into a polypeptide chain. Due to its unique role in gene expression, transcription is a primary point of gene regulation and consequently of crucial importance. Transcriptional regulation is achieved through the modification of all three phases of the transcription cycle: initiation, elongation and termination. Protein cofactors and regulatory signals encoded in the DNA sequence modulate the efficiency of these processes to control transcription. Despite 50 years of research on the mechanisms of transcription and its regulation, basic questions still remain unanswered.

In this dissertation, we employ optical tweezers in a single-molecule study of *Escherichia coli* RNAP. Single molecule measurements provide many advantages over conventional bulk assays that have traditionally been used for the analysis of transcription. Such bulk studies represent an ensemble average over 10^{12} or more molecules, which make the determination of low probability events or multiple populations difficult. Directly observing individual molecules overcomes these limitations, while still permitting the determination of ensemble properties through the ensemble of individual measurements.

Single-molecule measurements can also provide improved spatial and temporal resolution, as compared with conventional measurements. Employing optical trapping techniques to perform single-molecule measurements has the added benefit of permitting the application of load. A trivial consequence of applying load is the reduction of Brownian noise, which improves the resolution of the measurements. More importantly, the application of load can be used as a sensitive measure of displacement through the exponential dependence of kinetic rates on energy, the product of force and displacement. Optical tweezers therefore are well suited for the study of molecular motors and enzymes that translocate along their substrate, which for RNAP, is the DNA template.

Whereas the emphasis of this dissertation is the study of RNAP, several technical issues were considered before these measurements could be performed. The first chapter investigates the problem of optically induced damage in optical traps. In work that was a collaboration between Steven Block and Keren Bergman, and with the assistance of two undergraduate students: Edmund Chadd and Grace Liou, I investigated the wavelength dependence of optical damage in an optical trap. The major finding of this work was that optically induced damage could be prevented by removing oxygen from the preparation in which the trapping was carried out. This work has been published in the *Biophysical Journal* (Neuman, K. C., Chadd, E., Liou, G. F., Bergman K., and Block, S. M. (1999). Characterization of Photodamage to *Escherichia coli* in Optical Traps. *Biophysical Journal* 77, 2856-2863.) Shortly after this work was completed, Steve decided to move from Princeton to Stanford. In the process of rebuilding the optical trap that was used for the experiments on RNAP, several improvements were incorporated. These

improvements allowed the previously one-dimensional detection to be extended to a second dimension. The second chapter presents novel techniques and measurements that were made possible through two-dimensional detection. This work was done with a junior graduate student in the lab, Elio Abbondanzieri and will be submitted to the *Journal of Applied Physics*, or in a slightly modified form, as an *Optics Letter*. The third and final chapter presents single-molecule measurements of *Escherichia coli* RNAP that were made possible, in part, by aspects of the work presented in the first two chapters. This study was a collaboration between Steven Block, Jeff Gelles at Brandeis University and Robert Landick at the University of Wisconsin, Madison, conducted in Steve's lab with Elio Abbondanzieri. This work will be submitted to the journal *Cell* for publication.

Chapter 1

Abstract

Optical tweezers (infrared laser-based optical traps) have emerged as a powerful tool in molecular and cell biology. However, their usefulness has been limited, particularly *in vivo*, by the potential for damage to specimens resulting from the trapping laser. Relatively little is known about the origin of this phenomenon. Here, we employed a wavelength-tunable optical trap in which the microscope objective transmission was fully characterized throughout the near infrared, in conjunction with a sensitive, rotating bacterial cell assay. Single cells of *Escherichia coli* were tethered to a glass coverslip by means of a single flagellum: such cells rotate at rates proportional to their transmembrane proton potential (Manson et al., 1980). Monitoring the rotation rates of cells subjected to laser illumination permits a rapid and quantitative measure of their metabolic state. Employing this assay, we characterized photodamage throughout the near infrared region favored for optical trapping (790-1064 nm). The action spectrum for photodamage exhibits minima at 830 and 970 nm, and maxima at 870 and 930 nm. Damage was reduced to background levels under anaerobic conditions, implicating oxygen in the photodamage pathway. The intensity dependence for photodamage was linear, supporting a single photon process. These findings may help guide the selection of lasers and experimental protocols best suited for optical trapping work.

Introduction

"Optical tweezers," or optical traps, provide a unique means of manipulating and controlling biological objects (Svoboda and Block, 1994). Since the first demonstration of optical trapping by Ashkin (Ashkin, 1978; Ashkin et al., 1986), a host of applications have arisen in biology, both *in vivo* and *in vitro*. A drawback of optical trapping has been the damage induced by the intense trapping light. In practice, such damage limits the exposure time for trapped specimens, and has proved to be a significant problem for some optical trapping studies, particularly those *in vivo*. Indeed, Ashkin first encountered this problem and coined the colorful term "opticution" to describe the laser-induced death of specimens (Ashkin and Dziedzic, 1989). The potential for damage is readily appreciated by computing the light level at the diffraction-limited focus of a typical trapping laser: for a power of just 100 mW, the intensity is 10^7 W/cm^2, with an associated flux of 10^{26} photons/s·cm^2 (traps used in cell biology are generally based on lasers producing from 25 mW to 2 W in the specimen plane). Proposed mechanisms for photodamage include transient local heating (Liu et al., 1996), two-photon absorption (Berns, 1976; König et al., 1995; König et al., 1996a; Liu et al., 1996) and photochemical processes leading to the creation of reactive chemical species (Calmettes and Berns, 1983; Block, 1990; Svoboda and Block, 1994; Liu et al., 1996).

Some practical progress has been made towards decreasing photodamage in optical trapping systems, primarily through the choice of trapping lasers with wavelengths in the near infrared region (Ashkin et al., 1987). This corresponds to a waveband that is comparatively transparent to biological material, situated between the absorption bands of many biological chromophores in the visible, and the increasing

absorption of water toward longer wavelengths (Svoboda and Block, 1994). The most common source used in optical traps is the continuous-wave (CW) diode-pumped Nd:YAG laser (1064 nm) or its close relatives, Nd:YLF (1047 nm) and Nd:YVO_4 (1064 nm). These represent the most economical choices to achieve the requisite power (1-10 W) and output stability. But other sources suitable for optical trapping exist. Recent years have seen the emergence of high intensity, single-mode diode lasers, available in the wavelength region from 700-1500 nm, with powers up to ~1 W. Diode lasers possess exceptional amplitude stability, and are more economical than Nd-based lasers. Another option is the CW Ti:sapphire laser, which affords continuous tuning through much of the near infrared region (700-1000 nm) along with high output power. However, it requires a separate pump source, typically suffers reduced amplitude stability, and is far-and-away more costly than the alternatives. For now, Nd-based lasers continue to dominate the optical trapping field, but sources at other wavelengths may represent more advantageous choices for reducing photodamage

Berns and coworkers pioneered investigations of photodamage in optical traps using a variety of biological assays. Their work with temperature-sensitive fluorescent dye reporters in Chinese hamster ovary (CHO) cells and liposomes confirmed the prediction that local heating of micron-sized specimens is negligible from a tightly-focused CW laser source, thereby ruling out direct heating as a source of damage (Block, 1990, Liu et al., 1995, Liu et al., 1996). Additional studies, based on assaying the rates of chromosome bridge formation in rat kangaroo cells (Vorobjev et al., 1993), or cloning efficiency in CHO cells (Liang et al., 1996), established rough action spectra for damage over portions of the near infrared region. Following this work, additional studies, scoring

either CHO cell-cloning efficiency or loss of viability in human spermatozoa, led to the suggestion that damage is generated by a two-photon process (König et al., 1995; König et al., 1996a; Liu at al., 1996). In addition, work with fluorescent probes demonstrated no changes in the intracellular pH of trapped cells, and no detectable changes in DNA structure following CW laser illumination (as opposed to pulsed lasers, which do produce changes in acridine orange staining) (Liu et al., 1996).

While such experiments provide important clues to the photodamage process, the bioassays upon which they are based have certain intrinsic limitations. Chromosome bridge formation is largely qualitative and difficult to score. Cloning-efficiency and sperm-viability essentially provide a binary output (alive or dead), necessitating many measurements to gain adequate statistics. The assays are indirect, complex and time-consuming, requiring long incubation and/or growth periods, together with sensitive fluorescence-measuring capabilities. Furthermore, they do not readily lend themselves to continuously monitoring photodamage during experimental exposure.

To address these limitations, we employed a rotating bacterial cell assay that provides a quantitative, real-time measure of the metabolic state of the cell. The assay is based on attaching *E. coli* cells to a glass coverslip by means of a single flagellum (Block et al., 1982; Block et al., 1989). When the tethered cell turns its flagellar motor, the cell body is driven into rotation about its point of attachment, typically ~0-15 Hz, depending upon the cell size (and therefore on the load posed by viscous rotational drag). Motors of tethered cells spin at rates proportional to the transmembrane proton potential (Manson et al., 1980).

Although based on a prokaryote, this assay has some advantages over the eukaryotic systems employed previously. *E. coli* are robust and well-characterized organisms, which can be grown either aerobically or anaerobically, permitting evaluation of the role of oxygen in photodamage. Moreover, an enormous variety of mutants is available.

Using this assay, in conjunction with a broadly-tunable optical trapping system, we determined the action spectrum for photodamage from 790-1064 nm. This spectrum shows a roughly seven-fold variation in damage across this range, with two pronounced maxima at 870 and 930 nm. The least damaging wavelength was found to be 970 nm, followed closely by 830 nm. By growing and trapping cells in the absence of oxygen (or by removing oxygen after growth with a chemical scavenging system), we tested the effect of oxygen on the lifetime of cells. There was a significant increase in lifetime under anaerobic conditions: in fact, damage was reduced to nearly background levels. Determining photodamage as a function of laser power (at two different wavelengths, 870 and 1064 nm), we found that the sensitivity of cells (defined as the reciprocal of the lifetime) was linearly related to the intensity. These results suggest that photodamage in optical traps is mediated by oxygen, and that it involves a one-photon process.

Materials and Methods

Optics

The optical trap (schematic shown in Fig. 1.1) was based on three separate lasers: a Ti:sapphire ring laser tunable between 780 nm and 970 nm (model 899; Coherent, Inc., Santa Clara, CA), a MOPA diode laser at 991 nm (model 5762-A6; SDL, Inc., San Jose,

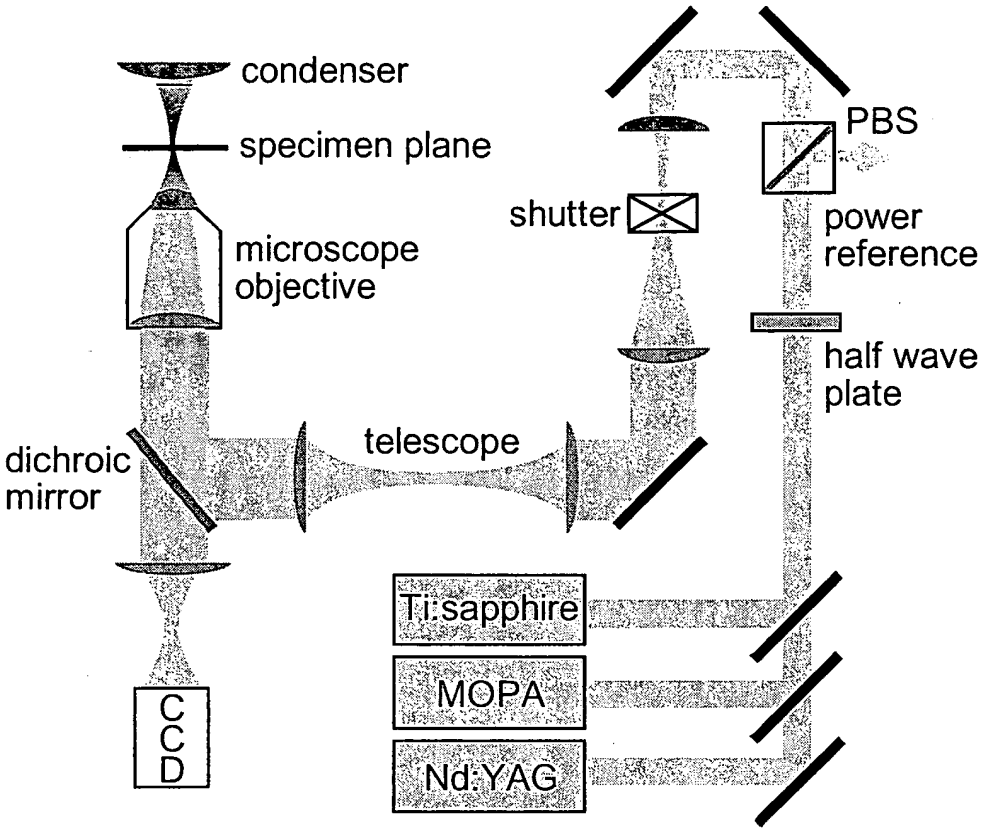

FIGURE 1.1. Simplified schematic of the tunable optical trap (not to scale). To cover the near infrared spectrum, one of three separate lasers was selected: the Ti:sapphire ring laser allows continuous tuning from 790 nm to 970 nm; the MOPA laser is at 991 nm; the Nd:YAG is at 1064 nm. The laser power is controlled via a rotatable halfwave plate and polarizing beam splitter (PBS). After the polarizer, the beam is expanded to slightly overfill the back pupil of the microscope objective. In the middle of the beam expander is a computer-controlled shutter. The laser is then directed into the epi-illumination path of an inverted microscope and reflected by a dichroic mirror into the microscope objective. The objective focuses the laser light to form a trap in the specimen plane and collects visible light from the condenser to form an image. The visible light passes through the dichroic mirror to a video camera (CCD).

CA) and a Nd:YAG laser at 1064 nm (model BL-106C; Spectra-Physics Lasers, Inc., Mountain View, CA). The Ti:sapphire laser was pumped with all lines from a large-frame Argon ion laser (Innova 400; Coherent, Inc., Santa Clara, CA). To insure true continuous-wave output from the Ti:sapphire laser, we incorporated an intercavity etalon (model 895; Coherent, Inc., Santa Clara, CA), which reduces the bandwidth and prevents temporal mode beating and partial modelocking (König et al., 1996a). The laser output was monitored in both temporal and frequency domains to check for pulses, which are indicative of temporal mode beating. Without the etalon, pulses were observed at a repetition rate of 186 MHz, corresponding to the round-trip time in the cavity. With the etalon in place, all mode beating ceased. The spatial mode of the Ti:sapphire laser and of the YAG laser was TEM_{00}, while the mode from the MOPA was slightly elliptical (ellipticity = 1.3). The output from the laser was expanded to slightly overfill the back pupil of the microscope objective: 63X/1.2 numerical aperture (NA) Plan NeoFluar, water/glycerol immersion (model 461832; Carl Zeiss, Inc., Oberkochen, Germany) and brought into an inverted microscope (Diaphot TMD; Nikon, Inc., Tokyo, Japan) via the epi-illumination port. The optical path included a computer-driven shutter (model 845; Newport Corp., Irvine, CA) controlling the laser trap. A dichroic mirror (model 635DCSPX; Chroma Technology Corp., Brattleboro, VT) in the microscope directed the laser into the objective while permitting the visible light, imaged by the objective, to pass through. Blue light artifacts induced by the microscope illumination source (50 W, 12 V DC halogen bulb) were minimized by placing a green interference filter (GIF; Nikon, Inc., Tokyo, Japan) in the illumination pathway.

Rotating, tethered cells were imaged on a CCD camera (model V-1056SX CCD; Video Runner, Inc., Culver City, CA). A time code generator (model TRG-50; Horita Co., Mission Viejo, CA) added a time stamp to the video signal, which was displayed on a B/W monitor (model PVM-97; Sony Corp., Montvale, NJ) and recorded by VCR (model AG-1980; Panasonic Co., Secaucus, NJ). In most cases, rotation rates of cells were simultaneously analyzed using a custom-built video cursor box placed in the video chain, which delivered a TTL pulse to a computer whenever the position of a rotating cell crossed a user-defined cursor position (Block and Berg, 1984). The same cursor box could also be used off-line with videotaped records of cells.

Microscope objective transmission calibration

To determine accurately the power delivered to the specimen plane, the transmission of the microscope objective must be characterized. Because of the high NA and short working distance of objectives used for optical trapping work, transmission cannot be measured by simply passing a beam of light through the lens and collecting it with an ordinary photodetector. Instead, the objective transmission as a function of wavelength was measured using a dual-objective technique (Misawa et al., 1991), as described by (Svoboda and Block, 1994). Measured transmission curves for several candidate objectives are displayed in Fig. 1.2.

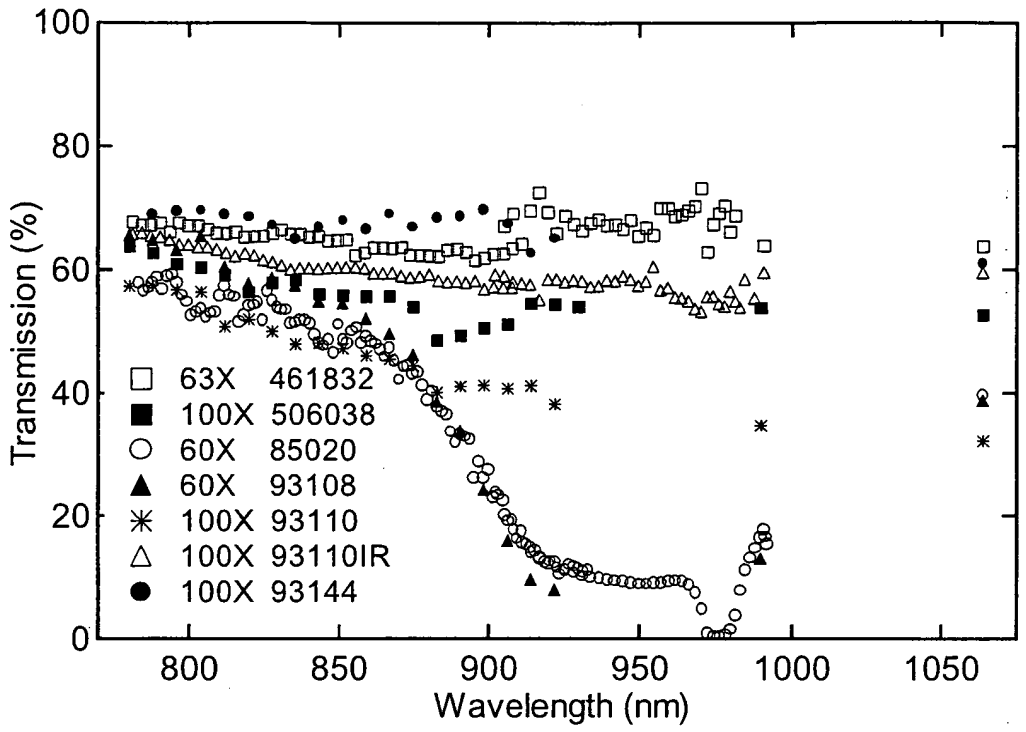

FIGURE 1.2. Microscope objective transmission curves. Transmission measurements were made with a dual-objective method (see Materials and Methods). Part numbers are cross-referenced in Table 1.1. The uncertainty associated with a measurement at any wavelength is ~5%.

Calibration of power in the specimen plane

The power in the specimen plane was determined by a multi-step procedure. First, the microscope objective used for optical trapping was replaced by a low NA objective with a known transmittance (20X/0.4 NA, model M-20X; Newport Corp., Irvine, CA; transmittance determined separately). A pyroelectric optical power meter (model LM-10; Coherent, Inc., Santa Clara, CA) was placed in front of this objective, at (or near) the specimen position, to record the intensity of light passing through. The power at this position, P_m, is related to the power delivered to the specimen plane in an actual experiment using a high NA objective, P_a, by $P_a = P_m \cdot T_1(\lambda)/T_2(\lambda)$ where $T_1(\lambda)$ is the measured transmission of the high NA objective and $T_2(\lambda)$ is the measured transmission of the low NA objective. (The entrance pupils of the low NA objective and the high NA objectives have the same diameter.) Next, to set the power at the specimen for any given wavelength, λ', the half wave plate in front of the polarizing beam splitter (PBS) was adjusted to obtain a reading of $P_m = P_a \cdot T_2(\lambda')/T_1(\lambda')$ on the optical power meter. The low NA objective was then replaced with the high NA trapping objective. Once the power was established in this way, any drift could be monitored via the second PBS port and corrected during an experiment. Power measurements as just described were performed prior to trapping in each experiment and after each change in the wavelength.

Bacterial assay

We employed a tethered cell assay (Block et al., 1982; Block et al., 1989) based on a strain of *E. coli* that carries two useful mutations (KAF95, a gift of Karen Fahrner, Harvard University; Berg and Turner, 1993). The first mutation is a deletion of the *cheY*

gene. CheY-P protein induces clockwise rotation of the flagellar motor: in its absence, cells rotate smoothly in the counterclockwise direction (Parkinson, 1978; Parkinson et al., 1983), facilitating measurements of rotation rates. The second mutation affects the flagellar protein, flagellin. In KAF95, the *fliC* gene encoding flagellin has an internal deletion leading to a non-specific binding interaction between flagella and the negative surface charge on the coverglass (Kuwajima, 1988). Cells carrying both these mutations spontaneously tether themselves and rotate continuously in the counterclockwise direction.

Cells of *E. coli* strain KAF95 were grown as described in (Block et al., 1982), except that cultures were grown in T-broth (10 mg ml^{-1} Bacto-Tryptone; Difco Laboratories, Detroit, MI; 5 mg ml^{-1} NaCl; Sigma, St. Louis, MO), supplemented with 100 μg ml^{-1} ampicillin (Sigma, St. Louis, MO) at 30° C, and the motility medium was that described in (Block et al., 1983). Cells were loaded into a flowcell consisting of a coverslip attached to a microscope slide by two pieces of double-sticky tape. Cells were allowed to tether for 10-15 minutes, after which time the flowcell was washed with 900-1200 μl of motility medium to remove untethered cells.

The experimental procedure was modified slightly to study cells under reduced oxygen tension. To insure anaerobic conditions, mineral oil (Fisher Scientific, Pittsburgh, PA) was layered over the surface of the growth medium prior to incubation to prevent oxygen from entering the test tube (cells consume any residual oxygen during the early stages of growth). The entire shearing and tethering process was carried out under nitrogen inside a glove bag, and the flowcell was sealed all around with vacuum grease (Apiezon M; M&I Materials Ltd., Manchester, England) before exposure to air. In other

experiments, anaerobic conditions were achieved by introducing an oxygen scavenging system into the flowcell after tethering but prior to trapping (250 μg ml^{-1} glucose oxidase, 30 μg ml^{-1} catalase, 4.5 mg ml^{-1} glucose; Sigma, St. Louis, MO). We estimate the time required to deplete the remaining oxygen in the flowcell under these conditions to be less than 1 s.

Tethered cells were held by the optical trap and periodically released to monitor their rotation rates (Fig. 1.3). In a typical experiment, once a suitably tethered cell was identified (initial frequency of 5-12 Hz), between 30 and 100 seconds of data were collected before the trap was turned on. Thereafter, during each successive ten-second interval, the cell was held for eight seconds by the trap and then released for two seconds. The rotation rate was determined from the timing of pulses generated by the video cursor box corresponding to full rotations (above). Pulses were captured by a data acquisition board (model AT-MIO-16E-10; National Instruments, Austin, TX), using a Labview program (Labview 4; National Instruments, Austin, TX), which was also used to control data acquisition and analyze rotation rates. Rotational data were further analyzed with Igor software (Igor Pro; Wavemetrics, Lake Oswego, OR). The data were smoothed, the start time (corresponding to when the trap was first turned on) was established, and the LD_{50} time, operationally defined as the time at which the rotation rate decreased to 50% of its initial value, was determined (see Fig. 1.4). Control data were obtained in a similar manner, but with cells exposed only to the microscope illumination. Experiments were performed at 25-27° C. A typical flowcell had 1-2 well-tethered cells per field of view (200 μm^2). After acquiring data from a cell, the next cell was chosen at least 400 μm away from the first. No more than two flowcells were made from a single culture. To

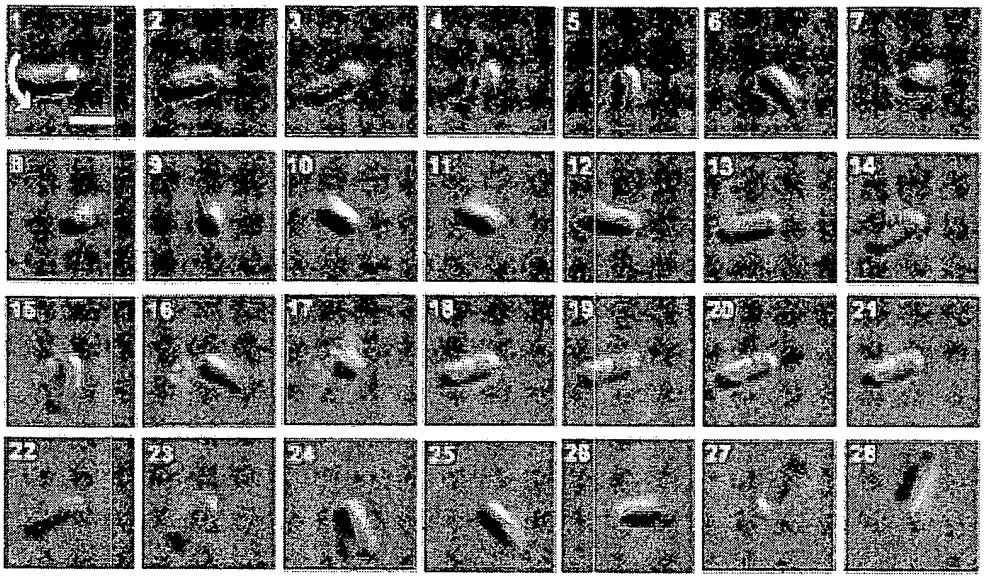

FIGURE 1.3. Images of a single rotating cell of *E. coli* tethered to a glass coverslip and imaged with DIC microscopy: successive video fields are displayed (time interval, 33 ms/field). The scale bar is 1 μm, the curved arrow indicates the direction of rotation, and the white dot shows the approximate center of rotation. The first 14 frames show the cell spinning freely (at ~2.5 Hz). The next 14 frames are with the trap on (the diffraction-limited laser focus is seen as concentric rings in frame 15). The cell rotates into, and is held by, the trap for four frames (18-21), before release (frame 22), after which it continues to rotate (frames 23-28).

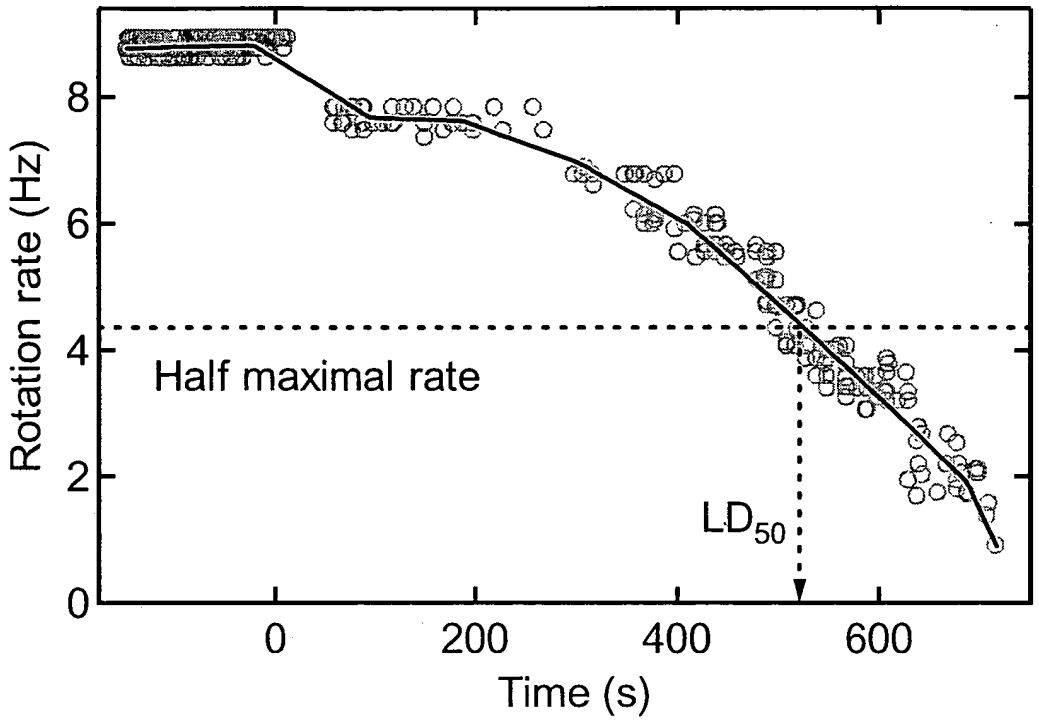

FIGURE 1.4. Rotation rate as a function of time for a single cell (open gray circles, experimental data; solid line, a linear spline fit to the data). The trap is turned on at t=0, after which there is a gradual decrease in rotation rate. The LD_{50} is depicted on the graph as the time at which the rotation rate decreased to 50% of the initial value. The appearance of layer lines in the data is a consequence of the video detection scheme, which requires an integral number of frames.

mitigate the effect of systematic variation in cell behavior from day to day, data for each point were collected from a minimum of three preparations over two days, with each point representing the average of 6 to 23 individual LD_{50} determinations. There was no correlation between initial rotation rate and LD_{50} time (correlation coefficient $r = 0.1$). We defined sensitivity as the inverse of the LD_{50} time. Data are presented as mean ± s.e.m.

Results

Microscope objective transmission calibration

Measured transmission data for seven high NA microscope objectives from three manufacturers are presented in Fig. 1.2 and Table 1.1. Overall transmission for the group varied from 1% to 73%. All objectives showed acceptable transmission in the short wavelength region of the infrared spectrum (~45-65%, ~790-830 nm). Beyond 850 nm, the transmission of most Plan Apo objectives fell dramatically, in certain cases to levels unacceptable for optical trapping work. However, objectives designed primarily for fluorescence work (Plan NeoFluar, Zeiss; Plan Fluor, Nikon), or explicitly for work in the near IR (93110IR, Nikon) had improved transmission characteristics in the longer wavelength region.

Wavelength-dependent damage

Control cells exposed to light from the microscope lamp, but not from the trapping laser, had an average LD_{50} time of 3300 ± 400 s with a corresponding sensitivity of $3.1 \times 10^{-4} \pm 0.4 \times 10^{-4}$ s^{-1}. The action spectrum (i.e., the wavelength-dependent

Part Number	Manu-facturer	Magnification/ Tube length (mm)/ Numerical aperture	Type designation	Transmission (±5%)			
				830 nm	850 nm	990 nm	1064 nm
461832	Zeiss	63/160/1.2 Water	Plan NeoFluar	66	65	64	64
506038	Leica	100/∞/1.4-0.7 Oil	Plan Apo	58	56	54	53
85020	Nikon	60/160/1.4 Oil	Plan Apo	54	51	17	40
93108	Nikon	60/∞/1.4 Oil	Plan Apo CFI	59	54	13	39
93110	Nikon	100/∞/1.4 Oil	Plan Apo CFI	50	47	35	32
93110IR	Nikon	100/∞/1.4 Oil	Plan Apo IR CFI	61	60	59	59
93144	Nikon	100/∞/1.3 Oil	Plan Fluor CFI	67	68	-	61

Table 1.1 Transmission of microscope objectives, cross-referenced with Fig. 1.2.

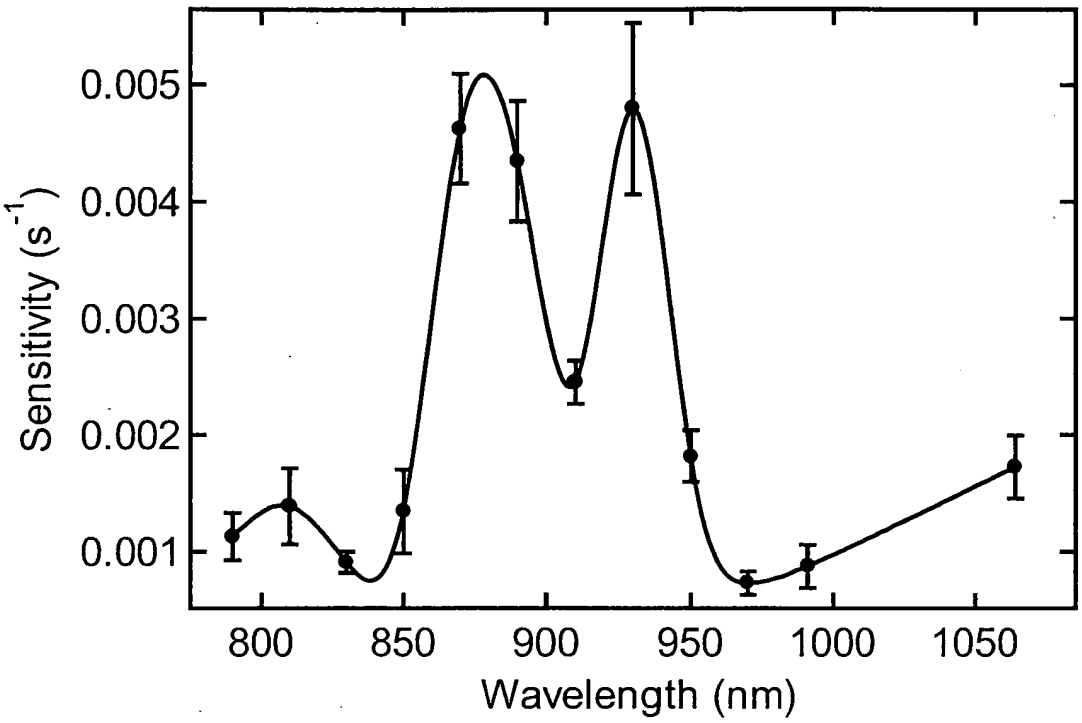

FIGURE 1.5. The action spectrum for *E. coli* trapped with 100 mW. Sensitivity is defined as the reciprocal of the average LD_{50}. (solid circles, experimental data; solid line, a cubic spline fit to the data). Each point represents an average of 12-23 determinations, with the errors shown (± s.e.m).

sensitivity) for *E. coli* trapped at 100 mW of laser power (determined in the specimen plane) is presented in Fig. 1.5. There was a roughly seven-fold difference between the most damaging wavelength (930 nm) and the least (970 nm). A direct comparison between the photodamage spectrum measured for *E. coli* and that reported by (Liang et al., 1996), based on cell cloning efficiency, is displayed in Fig. 1.6.

Oxygen dependent damage

A comparison between cells trapped under either aerobic or anaerobic conditions at two different wavelengths is presented in Fig. 1.7. Anaerobic conditions were achieved either by growing and maintaining cells in an oxygen free-environment or by introducing an oxygen scavenging system just prior to trapping. The experimental results were statistically identical in either case. The effect on photodamage of removing oxygen was dramatic, resulting in a three- to six-fold increase LD_{50}. Notably, trapping lifetimes under anaerobic conditions were the same as for the controls.

Intensity dependence of photodamage

Clues to the photochemical process underlying optical damage can be gained from the study of its intensity dependence. A simplified model for photodamage takes the form $S(P) = A + BP^n$, where S is the sensitivity, A is the control sensitivity, B is the wavelength-dependent sensitivity and P is the power. For a single photon-based process, n should be unity, while for a two-photon process, n should be two. A double-logarithmic plot of the reduced sensitivity, $S - A$, as a function of power at 870 and 1064 nm is plotted in Fig. 1.8. Data sets for each wavelength were fit to lines. At 1064 nm, the

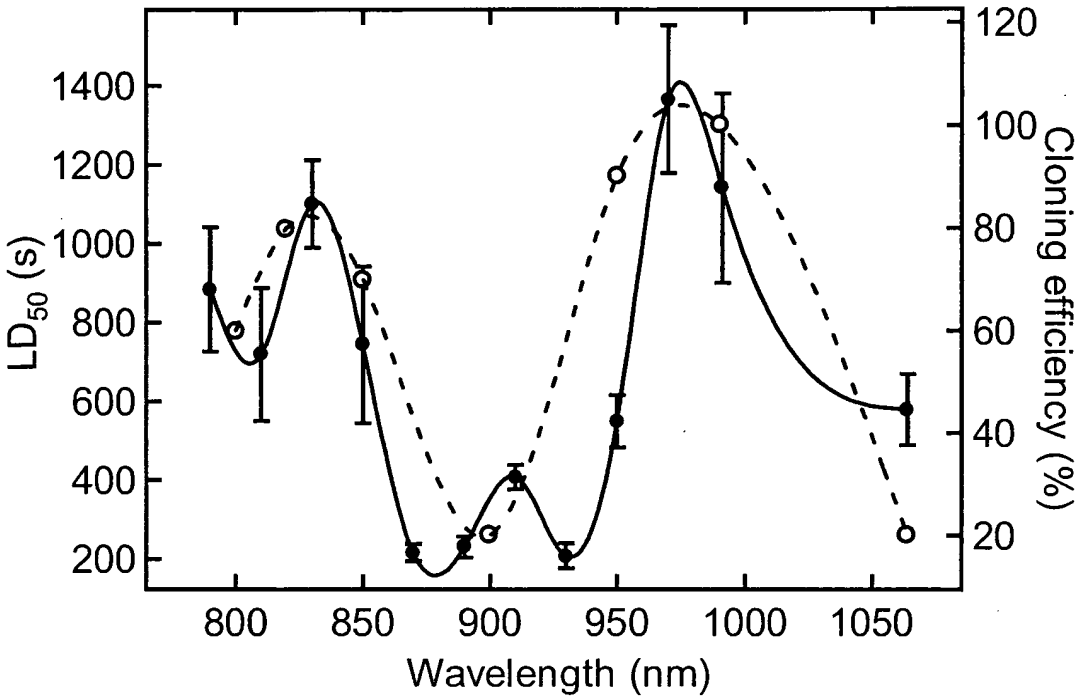

FIGURE 1.6. The wavelength dependence of photodamage in *E. coli* compared to CHO cells (solid circles and solid line, data replotted from Fig. 1.5 as LD_{50}, left axis; open circles and dashed line, right axis, cloning efficiency determined by Liang et al., 1996, *used with permission.* Lines represent cubic spline fits to the data). The cloning efficiency in CHO cells was determined after 5 min of trapping at 88 mW in the specimen plane (error bars unavailable), selected to closely match to our experimental conditions (100 mW in the specimen plane, errors shown as ± s.e.m).

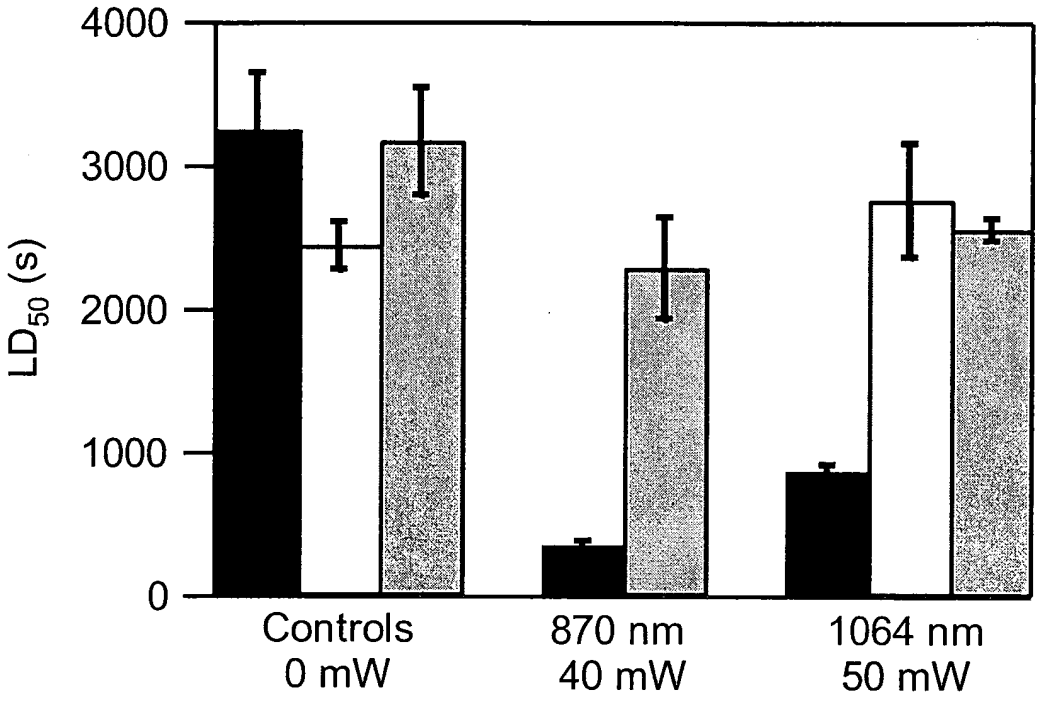

FIGURE 1.7. The oxygen dependence of photodamage. Comparison between *E. coli* cells trapped under aerobic and anaerobic conditions (solid bars, cells grown and maintained aerobically; open bars, cells trapped in the presence of an oxygen scavenging system; grey bars, cells that were grown and maintained anaerobically). Each point represents an average of 6-12 determinations, with the errors shown (± s.e.m).

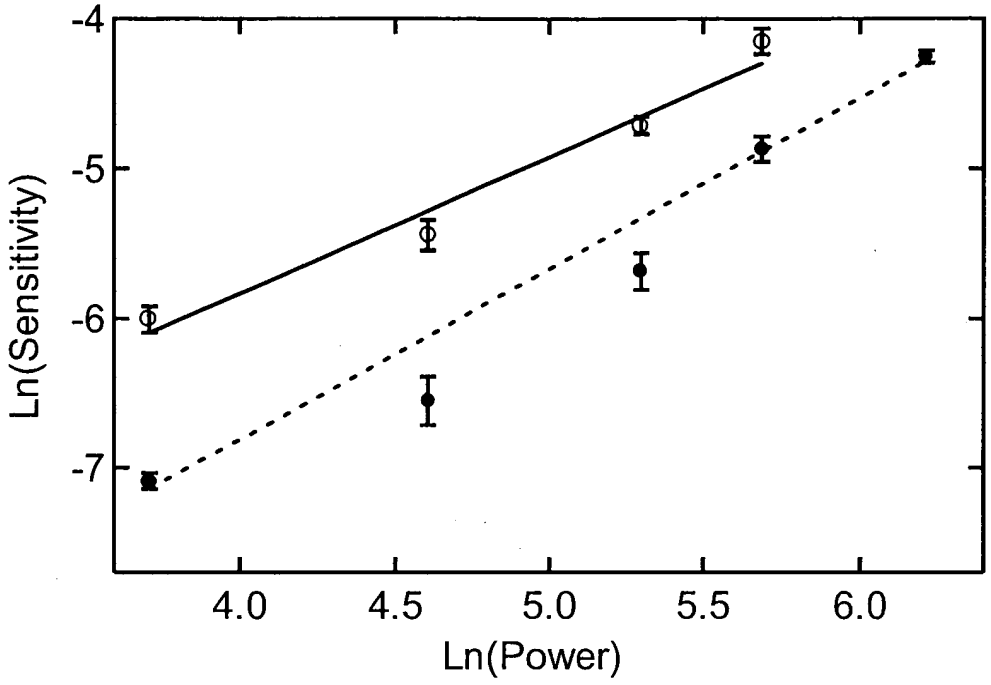

FIGURE 1.8. The intensity dependence of photodamage. Double logarithmic plot of the reduced sensitivity, *S-A*, versus power in the specimen plane at 870 nm (open circles; solid line) and at 1064 nm (filled circles; dashed line). The data are fit to lines, the slope of which gives the apparent order of the photodamage process. Fitted slope at 870 nm, 0.911 ± 0.06 (reduced $\chi^2 = 2.5$), slope at 1064 nm, 1.14 ± 0.03 (reduced $\chi^2 = 4.2$).

slope was 1.14 ± 0.03 (reduced $\chi^2 = 4.2$) while at 870 nm the slope was 0.91 ± 0.06 (reduced $\chi^2 = 2.5$). Taken together, the average slope is 1.06 ± 07, consistent with a linear, one-photon process.

Temporal dependence of photodamage

A distinct attribute of the rotating cell assay is an ability to obtain quantitative data from a single cell in real time, Fig. 1.4. Averaged single-cell curves for data taken at 870 nm with 100 mW are plotted in Fig. 1.9. To compute this average, individual curves were first normalized by their initial rotation rates and then the time was normalized by the measured LD_{50}. While there was considerable variation among individual curves, the average behavior displays an approximately linear decrease in rotation speed with time.

Discussion

The prominent features exhibited by the photodamage action spectrum (Fig. 1.5) are not easily understood. For example, the spectrum does not bear any superficial resemblance to the absorption spectrum of suspensions of *E. coli* cells, nor to water absorption (Palmer and Williams, 1974), nor to the absorption of molecular oxygen (Krupenie, 1972). The relatively sharp spectral features suggest that light is absorbed by one or more specific photopigments. However, our effort to match the observed spectrum with known chromophores was hampered by a dearth of spectral data for biological molecules in the near infrared region (most published spectra do not extend beyond ~750 nm). One noteworthy characteristic is the rough similarity between the wavelength dependence of photodamage seen in *E. coli* and in CHO cells (Fig. 1.6). This

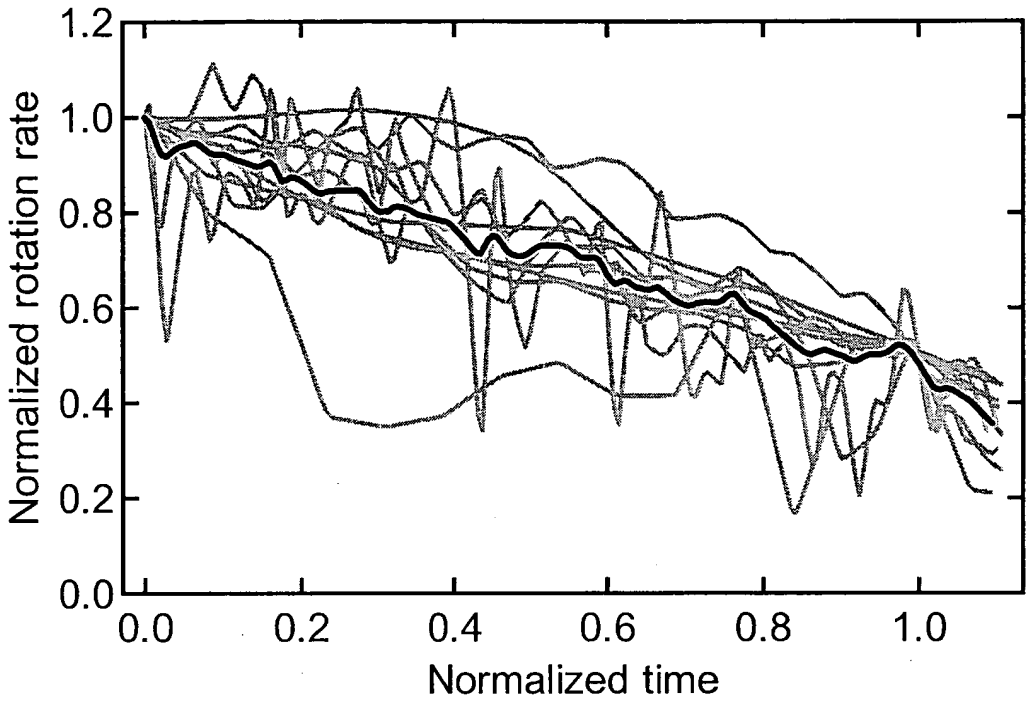

FIGURE 1.9. Photodamage as a function of time at 870 nm and 100 mW trapping power. Grey lines, normalized rotation rates versus normalized time. Rates were normalized according to their initial values, determined over an interval of ~30-100 s before the start of trapping at t = 0. Time was normalized according to the individual LD_{50} time determined for each cell, and typically ranged from ~200-300 s. Solid line, the unweighted average of these curves.

may indicate a common basis for damage in both prokaryotic and eukaryotic systems, possibly involving a ubiquitous intracellular chromophore, and suggests that it may be possible to generalize the present results, with caveats, to other organisms.

The dramatic increase in LD_{50} under anaerobic conditions (Fig. 1.7) implies a critical role for oxygen in the damage pathway. In its absence, trapped cells display a LD_{50} comparable to that of control cells. Whether oxygen is directly responsible, through the formation of a reactive oxygen species (the primary candidate being singlet molecular oxygen), or simply mediates the process, remains to be determined.

The nearly linear relationship between sensitivity and power strongly suggests that a single photon mechanism leads to photodamage (Fig. 1.8). This implies a direct absorption by some molecule (or molecules) in the infrared region, as opposed to a two-photon excitation mechanism in the visible (or UV) by unidentified fluorophores. This conclusion is at variance with previous reports implying a role for a two-photon process (König et al., 1995; König et al., 1996a; Liu et al., 1996), which were based on the finding that photodamage depended on the peak intensity, and not the average intensity, when using short-pulse laser irradiation (pulsed lasers are not normally used for optical trapping work). However, the clearest signature for a two-photon process is a quadratic dependence of damage on laser intensity, which was not explicitly established. One possible resolution of the discrepancy may be that there are two regimes for photodamage: at the extremely high peak intensities generated by mode-locked and Q-switched lasers (GW/cm^2; König et al., 1996a), photodamage may be dominated by some two-photon process, while at the lower intensities encountered in CW optical traps

(operating at MW/cm^2), the single photon mechanism prevails. An alternative explanation for the increased damage seen with pulsed lasers may be the onset of optoacoustic shockwaves (Hu, 1968; Bushanam and Barnes, 1975; Patel and Tam, 1981), which are pressure waves generated from high intensity light pulses focussed into a liquid medium. The overpressures produced can amount to several atmospheres, and may have deleterious effects. Optoacoustic damage has been studied in bulk tissues (Yashima et al., 1990; Yasima et al., 1991; Lustmann et al., 1992), but not in single cells.

The ability to continuously monitor single cells in the optical trap reveals the progress of the damage process. The nearly linear decline in rotation rate displayed by Fig. 1.9 was found for all wavelengths and laser powers investigated. Photodamage therefore seems to be a gradual process, not a catastrophic one. A damage threshold did not appear to exist. Even at the lowest power investigated, the rotation rate started to decrease immediately after trapping began.

A source of photodamage consistent with our data is the production of excited state (singlet) oxygen, mediated by a sensitizer molecule (Calmettes and Berns, 1983; Block, 1990; Svoboda and Block, 1994). Singlet oxygen is a long-lived, highly reactive species with well-established toxicity (Pryor, 1986; Dahl et al., 1987). While it is possible to produce singlet oxygen directly with laser illumination (Rosenthal, 1985), transitions from the ground state of molecular oxygen to the low-lying excited states are forbidden (Krupenie, 1972). Moreover, the absorption spectrum for molecular oxygen does not resemble the action spectrum for *E. coli*. Singlet oxygen may also be produced indirectly by exciting the triplet state of some sensitizer molecule, which in turn excites oxygen (Foote, 1976). It is conceivable, therefore, that the action spectrum for *E. coli*

matches the spectrum of an unidentified sensitizer. This conjecture is consistent with the observed reduction in damage when oxygen is removed from the sample, and by the relationship between intensity and damage. The lack of a damage threshold and its linear time course suggest that the toxic species may have a short lifetime (a longer-lived species that accumulated would be expected to produce damage at a rate that increased with time). Other possibilities exist. For example, the absorbing species could itself directly damage cells, independent of oxygen per se, but be present in concentrations that depended indirectly on the oxygen tension.

This work was motivated, in part, by a search for the most favorable wavelength for optical trapping in biological work. Based on these data, some general conclusions can be reached concerning the design of optical tweezers. Spectral transmission characteristics suggest that microscope objectives designed for fluorescence are better suited to optical trapping work than the (more costly) highly-corrected objectives designed for general high NA use. The large variation in throughput across the near infrared portion of the spectrum means that careful consideration should be given to transmission characteristics before selecting any objective for trapping work. We also note that our measurements of transmission for most of the objectives tested differed from the test data supplied by various manufacturers, with our figures invariably being lower by 10-30%. This difference may be attributable to their use of integrating spheres to measure transmission through high NA objectives, rather than the dual-objective method employed here. Integrating spheres do not distinguish between scattered and refracted light, and therefore count scattered rays, which do not contribute usefully to trapping.

The action spectrum (Figs. 1.5 and 1.6) suggests that the region between 870 and 910 nm is particularly damaging and should be avoided, especially for work *in vivo*. The least harmful wavelengths are 830 and 970 nm, which are about a factor of two less destructive than the 1064 nm Nd:YAG wavelength in common use. Currently, single mode diode lasers are available at all the favorable wavelengths, but only at relatively low power (typically, ~50-1000 mW). Continuing developments in diode laser technology may improve this situation, but there has been little increase in peak powers over the last four years. The fact that 970 nm is near the wavelength favored to pump erbium fiber lasers in the communications industry (980 nm) augurs well for the development of economical, hybrid diode-based designs that may eventually reach higher powers.

The dramatic increase in lifetime promoted by the removal of oxygen suggests that where possible, scavengers or other means should be employed to reduce the oxygen tension in trapping experiments. While this strategy works well for in vitro protein assays and anaerobic organisms, it is obviously untenable for work with most eukaryotes. For the latter, a useful approach may involve adding quenchers of singlet oxygen to media. These include simple amino acids (e.g., histidine, methionine, or tryptophan) and powerful anti-oxidant compounds such as β-carotene, DABCO (diazabicyclo [2,2,2] octane), or α-tocopherol (vitamin E). The trapped-and-tethered cell assay presented here should provide a ready means to test the protective potential of such compounds.

Acknowledgements

We thank Professor Steven Lyon for generously providing lab space, equipment and technical advice. We thank Professor Howard Berg for the generous loan of the video cursor box, and Dr. Karen Fahrner for the generous gift of strain KAF95. We thank the Princeton University Department of Chemical Engineering teaching lab for the use of their incubator. We are indebted to Drs. Lisa Satterwhite, Koen Visscher, and Mark Schnitzer for helpful discussions, Jason Hsu for preliminary work on this project, Anja Brau for assistance with the anaerobic data collection and Jeff Lehrman for assistance with LabView programming. We thank Neil Barlow of Micron Optics, Inc., for the loan of Nikon microscope objectives and Geoff Daniels of Leica America, Inc., for the loan of Leica objectives for transmission measurements. KCN was supported by a training grant from the NIH. SMB acknowledges support from grants from the NSF, NIH, and W. M. Keck Foundation.

References

Ashkin, A. 1974. Trapping of atoms by resonance radiation pressure. *Appl. Phys. Lett.* 19:283-285.

Ashkin, A., J. M. Dziedzic, J. E. Bjorkholm and S. Chu. 1986. Observation of a single beam gradient force optical trap for dielectric particles. *Opt. Lett.* 11:288-290.

Ashkin, A., J. M. Dziedzic and T. Yamane. 1987. Optical trapping and manipulation of single cells using infrared laser beams. *Nature.* 330:769-771.

Ashkin, A. and J. M. Dziedzic. 1989. Optical trapping and manipulation of single living cells using infra-red laser beams. *Ber. Bunsenges. Phys. Chem.* 93:254-260.

Berns, M.W. 1976. A possible two-photon effect in vitro using a focused laser beam. *Biophys. J.* 16:973-977.

Berg, H.C. and Turner, L. 1993. Torque generated by the flagellar motor of *Escherichia coli. Biophys. J.* 65:2201-2216.

Block, S. M., J. E. Segall and H. C. Berg. 1982. Impulse responses in bacterial chemotaxis. *Cell.* 31:215-226.

Block, S. M., J. E. Segall and H. C. Berg. 1983. Adaptation kinetics in bacterial chemotaxis. *J. Bacteriol.* 154:312-323.

Block, S. M. and H. C. Berg. 1984. Successive incorporation of force-generating units in the bacterial rotary motor. *Nature.* 309:470-472.

Block S. M., D. F. Blair and H. C. Berg. 1989. Compliance of bacterial flagella measured with optical tweezers. *Nature.* 338:514-518.

Block, S. M. 1990. Optical tweezers: a new tool for biophysics. *In* Foskett, J. K. and S. Grinstein (ed.). Noninvasive Techniques in Cell Biology *(Mod. Rev. Cell. Biol.* 9). Wiley-Liss, New York. 15:375-402.

Bushanam, G. S. and F. S. Barnes. 1975. Laser-generated thermoelastic shock wave in liquids. *J. Appl. Phys.* 46:2074-2082.

Calmettes, P. P. and M. W. Berns. 1983. Laser induced multiphoton processes in living cells. *Proc. Nat. Acad. Sci.* 80:7197-7199.

Dahl, T. A., R. A. Midden and P. E. Hartman. 1987. Pure singlet oxygen cytotoxicity for bacteria. *Photochem. Photobiol.* 46:345-352.

Foote, C. S. 1976. Photosensitized oxidation and singlet oxygen: consequences in biological systems. *In* Pryor, W. A. (ed.). Free radicals in biology, Volume II. Academic Press, New York. 85-133.

Hu, C. 1969. Spherical model of an acoustical wave generated by rapid laser heating in a liquid. *J. Acoust. Soc. Am.* 46:728-735.

König, K., H. Liang, M. W. Berns and B. J. Tromberg. 1995. Cell damage by near-IR microbeams. *Nature.* 377:20-21.

König, K., H. Liang, M. W. Berns and B. J. Tromberg. 1996a. Cell damage in near-infrared multimode optical traps as a result of multiphoton absorption. *Opt. Lett.* 21:1090-1092.

König, K., Y. Tadir, P. Patrizio, M. W. Berns and B. J. Tromberg. 1996b. Effects of ultraviolet exposure and near infrared laser tweezers on human spermatozoa. *Hum. Reprod.* 11:2162-2164.

Krupenie, P. H. 1972. The spectrum of molecular oxygen. *J. Phys. Chem. Ref. Data.* 1:423-520.

Kuwajima, G. 1988. Construction of a minimum-size functional flagellin of *Escherichia coli*. *J. Bacteriol.* 170:3305-3309.

Liang, H., K. T. Vu, P. Krishnan, T. C. Trang, D. Shin, S. Kimel and M. W. Berns. 1996. Wavelength dependence of cell cloning efficiency after optical trapping. *Biophys. J.* 70:1529-1533.

Liu, Y., D. K. Cheng, G. J. Sonek, M. W. Berns, C. F. Chapman and B. J. Tromberg. 1995a. Evidence for localized cell heating induced by infrared optical tweezers. *Biophys. J.* 68:2137-2144.

Liu, Y., G. J. Sonek, M. W. Berns, K. König and B. J. Tromberg. 1995b. Two-photon fluorescence excitation in continuous-wave infrared optical tweezers. *Opt. Lett.* 20:2246-2248.

Liu, Y., G. J. Sonek, M. W. Berns and B. J. Tromberg. 1996. Physiological monitoring of optically trapped cells: assessing the effects of confinement by 1064-nm laser tweezers using microfluorometry. *Biophys. J.* 71:2158-2167.

Lustmann, J., M. Ulmansky, A. Fuxbrunner and A. Lewis. 1992. Photoacoustic injury and bone healing following 193 nm excimer laser ablation. *Lasers Surg. Med.* 12:390-396.

Manson, M. D., P. M. Tedesco and H. C. Berg. 1980. Energetics of flagellar rotation in bacteria. *J. Mol. Bio.* 138:541-561.

Misawa, H., M. Koshioka, K. Sasak, N. Kitamura and H. Masuhara. 1991. Three dimensional optical trapping and laser ablation of a single polymer latex in water. *J. Appl. Phys.* 70:3829-3836.

Palmer, K. F. and D. Williams. 1974. Optical properties of water in the near infrared. *J. Opt. Soc. Am.* 64:1107-1110.

Parkinson, J. S. 1978. Complementation analysis and deletion mapping of *Escherichia coli* mutants defective in chemotaxis. *J. Bacteriol.* 135:45-53.

Parkinson, J. S., S. R. Parker, P. B. Talbert and S. E. Houts. 1983. Interactions between chemotaxis genes and flagellar genes in *Escherichia coli. J. Bacteriol.* 155:265-274.

Patel, C. K. N. and A. C. Tam. 1981. Pulsed optoacoustic spectroscopy of condensed matter. *Rev. Mod. Phys.* 53:517-550.

Pryor, W. A. 1986. Oxy-radicals and related species: their formation, lifetimes, and reactions. *Ann. Rev. Physiol.* 48:657-667.

Rosenthal, I. 1985. Chemical and physical sources of singlet oxygen. *In* Frimer, A. A. (ed.). Singlet O_2 ,Volume I, physical and chemical aspects. CRC Press, Boca Raton. 13-38.

Schnitzer, M. J. and S. M. Block. 1997. Kinesin hydrolyses one ATP per 8-nm step. *Nature.* 388:386-390.

Svoboda, K. and S. M. Block. 1994. Biological applications of optical forces. *Annu. Rev. Biomol. Struct.* 23:247-285.

Vorobjev, I. A., H. Liang, W. H. Wright and M. W. Berns. 1993. Optical trapping for chromosome manipulation: a wavelength dependence of induced chromosome bridges. *Biophys. J.* 64:533-538.

Yashima, Y., D. J. McAuliffe, T. J. Flotte. 1990. Cell selectivity laser induced photoacoustic injury of skin. *Lasers Surg. Med.* 10:280-283.

Yashima, Y., D. J. McAuliffe, S. L. Jacques, T. J. Flotte. 1991. Laser-induced photoacoustic injury of skin: effect of inertial confinement. *Lasers Surg. Med.* 11:62-68.

Chapter 2

Introduction

Since the invention of the single beam optical trap by Ashkin and co-workers, (Ashkin, 1970; Ashkin, 2000; Ashkin et al., 1986) most applications have been limited to applying force and measuring displacement in the lateral dimension (Greulich, 1999; Mehta et al., 1998; Svoboda and Block, 1994a; Visscher and Block, 1998; Visscher et al., 1996; Wright et al., 1990). Axial motion within the optical trap has been determined by measuring the intensity of scattered laser-light on an overfilled photodiode (Friese et al., 1999; Ghislain et al., 1994; Ghislain and Webb, 1993; Peters et al., 1998), through two-photon fluorescence generated by the trapping laser (Florin et al., 1996; Florin et al., 1997; Jonas et al., 2001; Stelzer et al., 1998; Zhang et al., 1998), and by evanescent-wave fluorescence at the surface of a cover slip (Clapp et al., 1999; Sasaki et al., 1997). Whereas these techniques provide sensitive axial position determination, they also require integration of additional detectors, and in some cases, fluorescence capabilities into an optical trapping instrument. Consequently, these techniques have not been widely adopted. The axial position of a trapped particle can also be determined from the normalized total detection laser intensity in the back focal plane of the objective (Pralle et al., 1999b; Rohrbach and Stelzer, 2002b). The axial position signal arises from the interference between light scattered by the trapped particle and the unscattered beam, which has an axial-position dependent Gouy phase shift through the focus. An analogous description of the lateral position signal of a quadrant photodiode in the back focal plane has been described (Allersma et al., 1998; Gittes and Schmidt, 1998). A simple extension of quadrant photodiode-based lateral position detection can provide axial position

detection by recording and appropriately normalizing the total incident intensity on the position detector.

The ability to accurately measure axial displacements in the trap necessitates a better understanding the absolute position of a trapped object with respect to the surface of the slide or flow cell. Absolute axial measurements are particularly important when the trapped particle is physically connected to the surface, as is often the case in biological applications. Improvements in piezoelectric stage design make accurate and precise three-dimensional positioning possible, but location of a trapped particle relative to the surface remains uncertain. Compounding the problem is the focal shift that arises from focusing through an interface between mismatched indices of refraction (Fig 2.1 A). The focal shift introduces a scaling factor between the axial motion of the cover glass and the focus. the focal shift is difficult to calculate and harder to measure due to the high numerical aperture (NA) of the objectives required for optical trapping. Absolute axial position determination has previously been addressed via evanescent wave fluorescence (Sasaki et al., 1997), through the analysis of interference or diffraction patterns captured with video (Gosse and Croquette, 2002; Radler and Sackmann, 1992), or through the hydrodynamic drag on the trapped particle as it approaches the surface(Wang et al., 1997). These techniques suffer from the short range of detectable motion for the fluorescence-based methods, and by the slow temporal response for video and drag-force-based measurements.

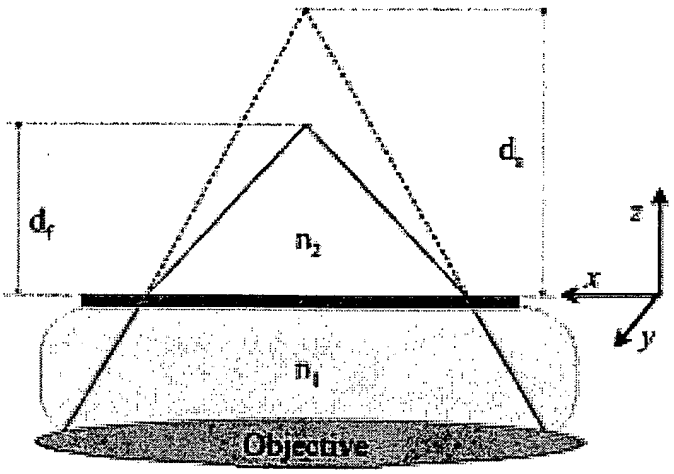

Figure 2.1 A. Illustration of the focal shift that occurs on focusing light through the interface between two mismatched indices of refraction. Convergent light from the objective travels into index n_1, through the interface between n1 and n2 (n1>n2) and comes to a focus at position df above the interface. Position ds is where the focus would be in the absence of an index mismatch. i.e. if the light were focused in a medium of n1 alone. The fractional focal shift, df/ds is constant. The coordinate system on the right defines the axes and directions throughout the paper. Light propagates in the positive *z* direction. The cover slip (heavy line between n1 and n2) is attached to the microscope stage. Negative axial motion of the stage moves the focus point further from the surface.

We have implemented axial detection with an interferometric lateral position detector in which the intensity at the photodiodes is normalized by the incident laser intensity to obtain the axial position signal. The two-dimensional (one axial and one lateral dimension) detector has been employed to determine the relationship between axial and lateral stiffness and to measure the change in lateral stiffness as a function of axial position in the optical trap. Furthermore, we demonstrate a simple procedure for finding the surface of the trapping chamber and absolute positioning of a trapped particle. The high signal to noise ratio achieved by normalizing the intensity at the detectors permitted the detection of a secondary interference effect due to multiple light scattering from the trapped particle and the glass-water interface interfering with the unscattered beam. Comparisons of observed traces are presented with numerical results of the scattering and interference of light from a sphere near a surface. Spatial periodicity of multiply scattered interference signals provides a sensitive measure of the focal shift. Calculated focal shifts are found to overestimate measured focal shifts.

Results and discussion

The optical layout detection scheme are displayed in Fig. 2.1B. An existing optical trap (Svoboda and Block, 1994b; Wang et al., 1997) was modified by adding a normalizing detector monitoring the bleed-through of the trapping laser on a dielectric mirror and a feedback-stabilized three-axis piezoelectric stage (Physik Instrumente, P-517.3CD) to which the trapping cell was affixed. The optical trap was built around an inverted microscope (Carl Zeiss Axiovert 35) with a polarized ND:YLF trapping laser (TFR,

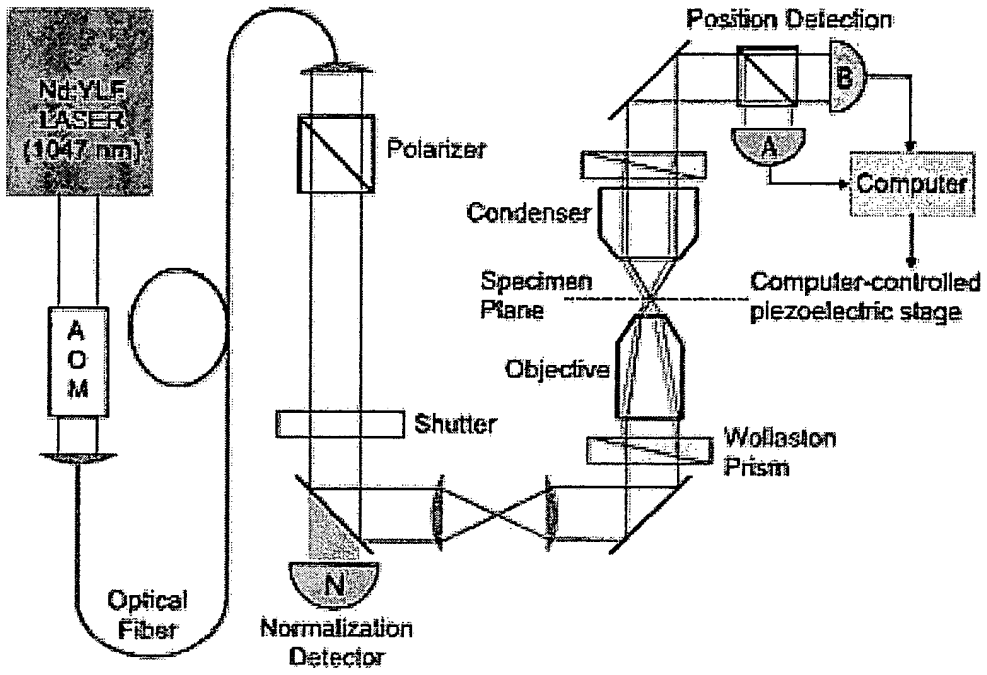

Figure 2.1B. The optical trapping interferometer. Light from a ND:YLF laser passes through an acoustic optical modulator (AOM) that is used to adjust the intensity. After the AOM, the light is coupled into a single-mode polarization-maintaining optical fiber. On the output of the fiber, the light passes through a polarizer to ensure a single polarization, through a 1:1 telescope and into the microscope where it passes through the Wollaston prism and is focused in the specimen plane. The scattered and unscattered light is collected by the condenser, is recombined in the second Wollaston prism, the two polarizations are split in a polarizing beam splitter and are detected on two photodiodes (A and B). The bleed-through on a turning mirror is measured by a photodiode (N) to record the instantaneous intensity of the laser. The signals from the two detector photodiodes and the normalization diode are digitized and saved to disk.

Spectra physics ;λ=1047 nm 2.5 W, TEM_{00}) that is focused to a diffraction-limited spot by an objective (Carl Zeiss Plan Neofluar 100X, 1.3 N.A. oil). The trapping laser passes through a Wollaston prism below the objective producing two orthogonally polarized and spatially separated spots in the specimen plane, which act as a single trap. A trapped object located asymmetrically between the two spots produces a relative phase shift between the two beams. Motion of the trapped particle along the Wollaston shear axis can be determined from the ellipticity of the recombined light in the back focal plane of the condenser. The recombined light passes through a quarter-wave plate and a polarizing beam splitter. Two photo detectors measure the power in each polarization. The difference between the photo detector signals normalized by their sum is a measure of the motion of the particle along the Wollaston axis (Denk and Webb, 1990). The sum of the detector signals normalized by the incident laser power provides axial position information (Pralle et al., 1999; Rohrbach and Stelzer, 2002). Modulation representing the axial position signal amounted to only a small fraction of the total intensity and was of the same order of magnitude as intensity noise of the laser. Normalizing the axial position signal with reference to the instantaneous incident laser power, therefore, provided a significant improvement in the signal to noise ratio.

Experiments were performed with polystyrene beads (diameter 500 ± 13 nm; Bangs laboratories) suspended in distilled water or stuck to the surface of the flow cell (#1.5 glass coverslip; Corning) in 400 mM KCl. Flow cells were constructed by forming a ~0.5 cm channel with two pieces of double sticky tape (~100 μm thick; 3M) on a microscope slide to which a coverslip was attached.

Calculations were performed with an objective NA of 1.3, an immersion oil index of refraction of 1.515, and a laser wavelength of 1047 nm. The trapping medium had an index of refraction of 1.33 for water and 1.4 for a 50% mixture of water and glycerol. The polystyrene beads had an index of 1.57.

Traces of axial position for trapped and stuck beads as the coverslip was moved in the axial direction are shown in Fig. 2.2. The trace for the stuck bead reflects the axial position signal of a particle in the trap. As the bead was moved through the focus of the laser (marked on the figure), the phase of light scattered from the bead changed by 180 degrees relative to the unscattered light resulting in the modulation of intensity. The region between the extrema of the stuck-bead curve was well described by the expression for the axial sensitivity derived by Pralle et al.,1999:

$$\frac{I_z}{I}(z) \propto \left(1+\left(\frac{z}{z_0}\right)^2\right)^{1/2} \sin(\arctan z/z_0) \qquad (2.1)$$

Where the overall scaling factor has been ignored. z is the axial displacement from the beam waist and $z_0 = \pi w_0^2/\lambda$ is the Raleigh length of the focus. The fit returned a value for the beam waist, $w_0 = 0.436$ μm. A two-dimensional position calibration was acquired by raster scanning a stuck bead in the axial dimension and along the Wallaston shear axis while recording the lateral and axial position signals. The secondary peak at ~-3000 nm is possibly due to the bead passing through a secondary maximum preceding the focus, which arises from the index mismatch between glass and water (Wiersma et al., 1997).

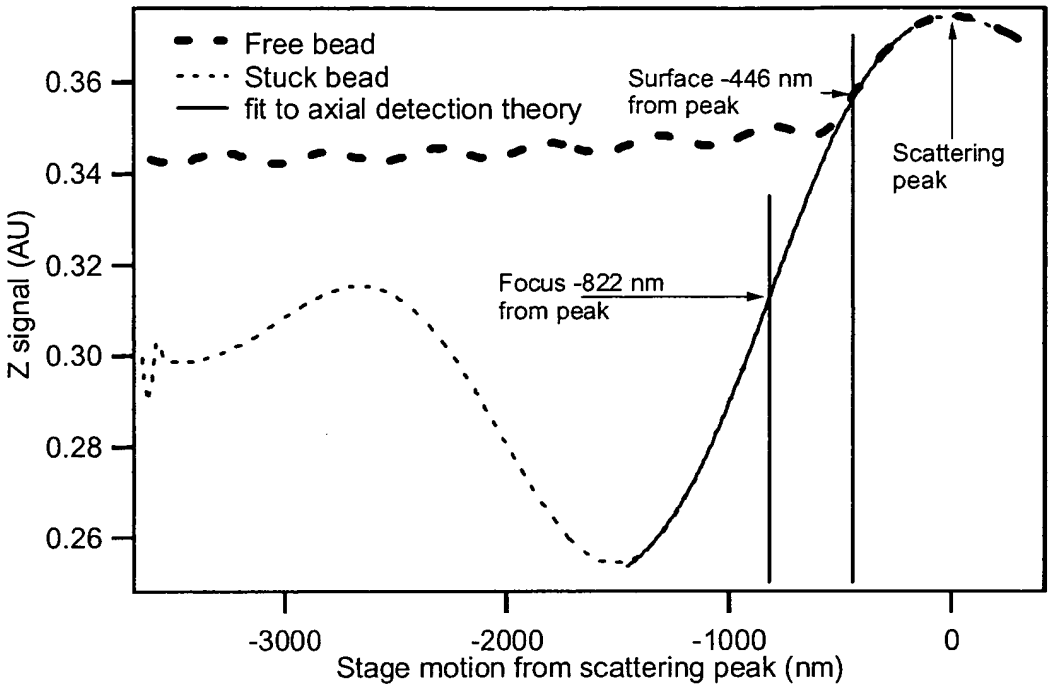

Figure 2.2. Axial position signals for a free (heavy dashed line) and stuck (light dashed line) bead as the stage was scanned in the axial direction. All stage motion is relative to the scattering peak, which is indicated on the right of the figure. The positions of the surface (measured) and the focus (calculated) are indicated by vertical lines on the figure. The axial detection fit (Equation 2.1) to the stuck bead trace is shown in the region around the focus as a heavy solid line.

As the trapped bead was brought toward the surface, a slight periodic modulation of the axial position signal was apparent. When the trapped bead began to interact with the coverglass the free and stuck bead signals merged and eventually became indistinguishable. The approximate location of the surface in relation to the laser focus was determined by finding the point at which both curves merged. Brownian motion of the trapped bead will shift this point slightly in a stiffness dependent manner and will introduce a large uncertainty in the position of the surface. The scattering peak in Fig. 2.2, however, serves as an easily identified fiducial reference from which the trapped bead can be moved an absolute distance by moving the stage. In this manner, trapped particles can be reproducibly positioned at a fixed but unknown distance relative to the surface. In order to obtain the precise location of the trapped particle above the surface, the position of the scattering peak with respect to the surface and the fractional focal shift must be determined.

The position of the scattering peak with respect to the coverslip surface and the fractional focus shift can be determined by a one time measurement of the drag on a trapped bead at a series of positions above the scattering peak. The interaction of a sphere with the boundary layer of water near a surface increases the hydrodynamic drag β in a calculable manner, known as Faxen's law (Svoboda and Block, 1994a):

$$\beta = \frac{6\pi\eta a}{\left[1 - \frac{9}{16}\left(a/h\right) + \frac{1}{8}\left(a/h\right)^3 - \frac{45}{256}\left(a/h\right)^4 - \frac{1}{16}\left(a/h\right)^5\right]} \qquad (2.2)$$

which depends only on the bead radius a the distance above the surface h and the kinematic viscosity of the liquid η. By measuring the roll-off frequency or the displacement of the trapped bead as the stage is oscillated, the drag force can be determined at different stage positions relative to the scattering peak and normalized by the calculated asymptotic value, the Stokes drag relation, $6\pi\eta a$. The resulting curve (Fig. 2.3) was completely described by two parameters: a scaling parameter that represents the fractional focal shift and an offset parameter indicative of the distance between the scattering peak and the coverglass surface. The fit parameters from the curve in Fig. 2.3 allow the absolute positioning of a trapped particle in the axial direction with respect to the coverglass with an uncertainty of 3%. The position of the surface calculated in this manner is indicated in Fig. 2.2. The fractional focal shift was 0.82 ± 0.02 i.e. the position of the laser focus changes by 82% of the stage motion.

Two-dimensional position detection permits measurement of the axial stiffness and mapping of the lateral stiffness as a function of axial position in the trap. Due to the refractive index of the polystyrene bead, there is a large scattering force in the axial direction. Consequently, the equilibrium axial position of the bead in the optical trap is above the focus, where the lateral intensity gradient and hence the lateral stiffness are reduced from their values at the focus. In experiments where the bead is displaced from the axial equilibrium position, the lateral trapping stiffness can change significantly. Changes in lateral stiffness as a function of axial position in the trap were determined using beads tethered with DNA to the surface of the flow cell (Fig. 2.4 inset). Avidin-

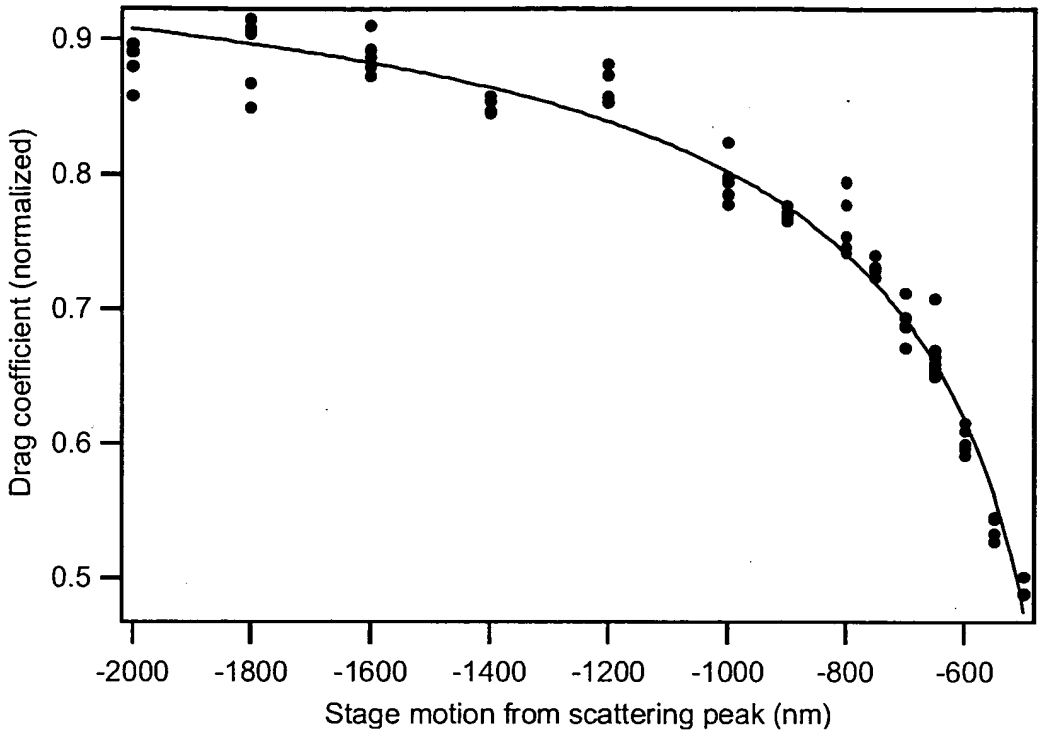

Figure 2.3. Normalized drag coefficient as a function of distance from the scattering peak. The drag coefficient (dots) was determined through roll-off measurements and from the displacement of a trapped bead as the stage was oscillated. The normalized drag coefficient was fit to Faxen's law (Equation 2.2) (solid line) with a height offset and a scaling parameter as the only free parameters.

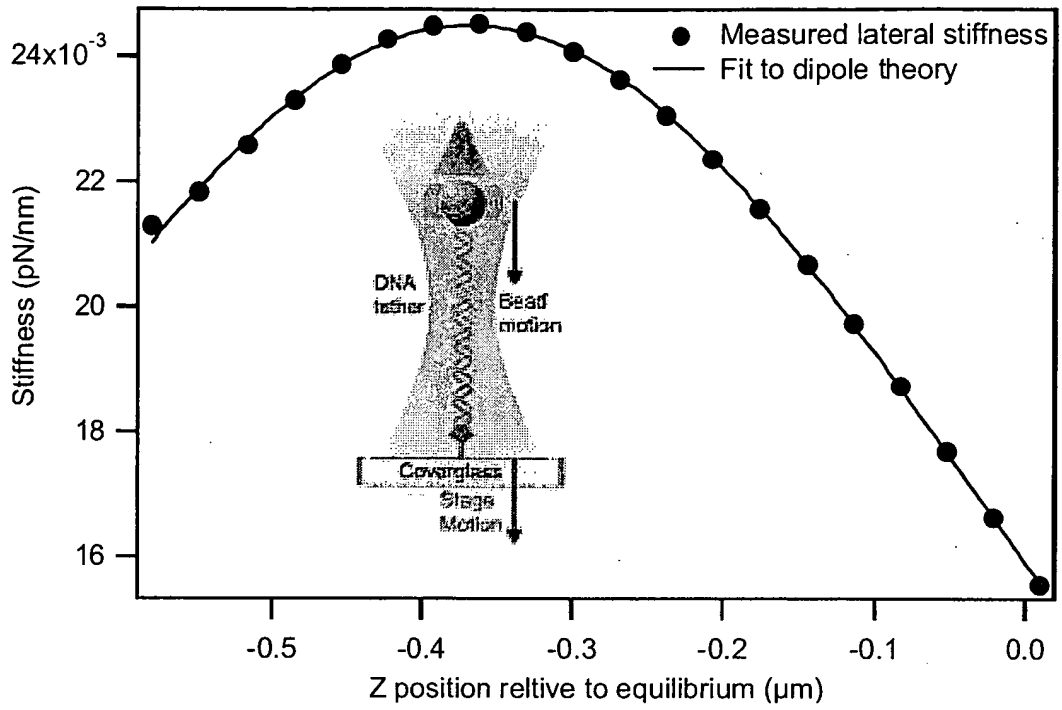

Figure 2.4. Axial dependence of lateral stiffness. The experimental geometry for this measurements is depicted in the inset. A polystyrene bead was tethered to the surface of the cover glass through a long DNA tether. The stage was moved in the negative axial direction, which pulls the bead towards the laser focus, and the lateral stiffness was determined by measuring the lateral variance of the bead. The data (dots) are fit with the expression for a simple dipole particle (Equation 2.3) with the power in the specimen plane, the beam waist and an axial offset as free parameters.

coated beads were prepared and mixed with biotin-labeled DNA (1.66 μm in length) in a 3:1 ratio, ensuring that less than 5% of the beads had multiple DNA molecules attached. The DNA was tethered to the surface of the flow cell via a digoxigenin link on the free end of the DNA that in turn was bound by a digoxigenin antibody on the surface. Tethered beads were trapped, the attachment point of the tether was determined and was centered on the optic axis. The bead was then pulled through the trap in the axial dimension by lowering the stage in 20 nm increments. At each position, the stiffness of the trap was ascertained through the variance method (Svoboda and Block, 1994a). The contribution of the axial force to the lateral stiffness was calculated by treating the tethered bead as a simple pendulum. Axial stiffness was found to be eight-fold less than the lateral stiffness, which, in conjunction with the long tether, resulted in a maximal increase in lateral stiffness of 3%. The average of 12 such measurements is shown in Fig. 2.4, along with a fit to the lateral stiffness based on a simple dipole and zero order Gaussian beam model (Harada and Asakura, 1996).

$$S_z = \frac{8n_2 p}{cw_0}\left(\frac{a}{w_0}\right)^3\left(\frac{m^2-1}{m^2+2}\right)\left(1+\left(\frac{z}{z_0}\right)^2\right)^{-2} \qquad (2.3)$$

Where n_2 is the index of refraction of the medium, p is the laser power in the specimen plane, c is the speed of light, a is the radius of the particle, and m is the ratio of the indices of refraction of the bead and the medium. W_0, z and z_0 are the beam diameter at the waist, the axial displacement of the particle relative to the focus and the Raleigh range, respectively, as previously defined.

The fit was quite good except that the intensity was a factor of six less than the estimated intensity in the specimen plane. This discrepancy was to be expected, as it has been

shown that for large particles the dipole approximation overestimates the stiffness (Harada and Asakura, 1996). The other two parameters of interest are the beam waist and the equilibrium axial position of the bead in the trap. The fit returned values of 0.433 μm for the beam waist and 0.368 μm for the displacement of the bead from the focus. These compare quite well with the values determined from the fit to the axial position signal, which were 0.436 μm and 0.379 μm respectively. The change in lateral stiffness between the equilibrium position and the focus was substantial; a factor of 1.5 for the geometry and beads studied.

To understand the origin of the secondary interference observed in the axial position signal as a trapped bead is moved relative to the surface (Fig. 2.2), we numerically solved the scattering of light from a sphere near a surface following the solution obtained by Videen (Videen, 1991; Videen, 1993). The scattered field was combined with the unscattered field of a Gaussian focus in the far field, following the work of Gittes and Schmidt (Gittes and Schmidt, 1998). The intensity was calculated and integrated over the collection angle of the condenser. These calculations make several simplifying assumptions: (1) The incident field on the sphere is a linearly polarized plane wave, rather than a Gaussian field, the phase and intensity of the plane wave, however, were adjusted to match those of a Gaussian beam that was further presumed to impinge on the surface at normal incidence. (2) The zero order Gaussian approximation was made for the unscattered light, which fails to completely describe the fields of light focused with a high NA objective. (3) The fields scattered by the sphere that reflect off the surface and interact with the sphere impinge on the surface at near normal incidence. This is a

relatively minor assumption that was included in the original paper (Videen, 1993). Several representative axial position scans of trapped beads recorded with decreasing condenser NAs are shown in Fig. 2.5 A. For comparison, the theoretical intensity from the extended Videen solution is presented in Fig. 2.5 B. The qualitative features of the theoretical curves reproduce the measured traces, however the theory fails to predict absolute quantitative aspects of the data. The predicted amplitude of intensity modulation is less than the measured amplitude. More importantly, the slight rise in baseline intensity as the bead approaches the surface is completely absent from the calculated curves, particularly at low condenser NAs. These discrepancies may arise from the simplifying assumptions, which are only poorly satisfied in the case of a high NA focus, or they may arise from experimental conditions that were not accounted for in the theoretical treatment. Nevertheless, the agreement between theory and experiment is sufficient to conclude that the observed intensity modulation arises from the multiple scattering of light between the bead and the surface.

As the NA of the condenser decreased, intensity modulation became more regular and persisted over longer distances. For such small collection angles and uniform intensity modulation patterns, the modulation can be understood as a simple etalon effect. The backscattered light from the trapped bead reflects off the surface and interferes with the forward scattered and unscattered light in the back focal plane of the condenser. The phase difference between these two fields includes a constant term that arises because of

the Gouy phase and a term that depends on the separation between the bead and the surface. The spatial frequency of the intensity modulation is: $d=\lambda_n/2 = \lambda/2 \cdot n$, where d is

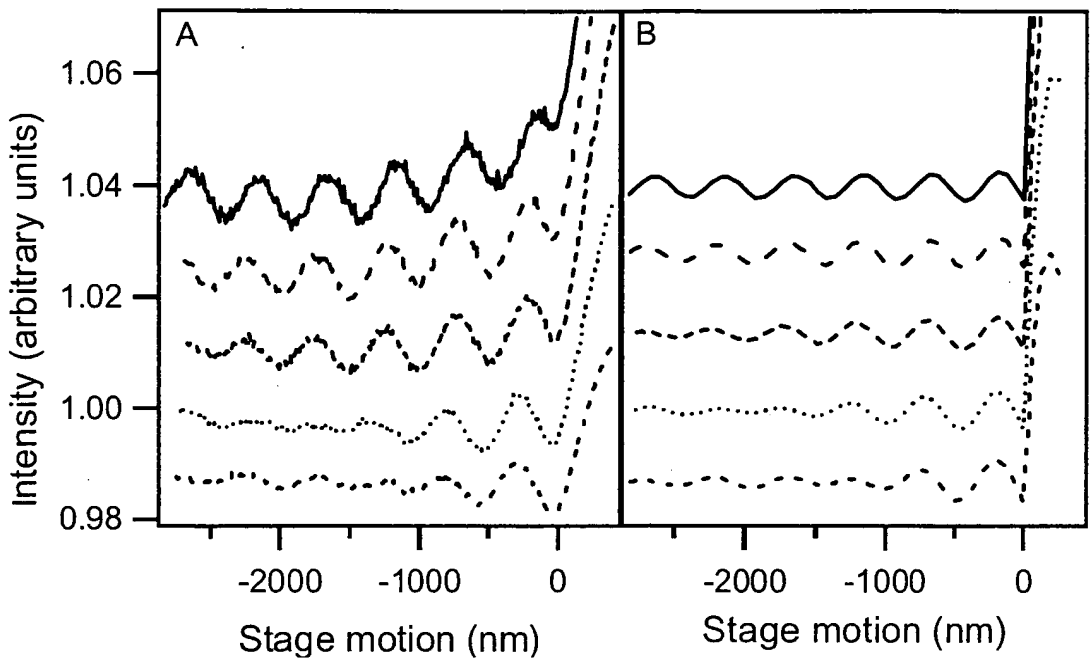

Figure 2.5. Comparison between measured (A) and simulated (B) axial position signals of trapped beads at different condenser collection angles. Axial position signals were measured as a trapped bead was moved relative to the cover slip for a series of different iris aperture stops (A). The traces are arranged in order of decreasing iris aperture from bottom to top and have been shifted on the *y*-axis for clarity. For comparison, simulated position signals for collection angles estimated from the measured traces are displayed on the right (B). The simulated traces reproduce the gradual decay of the interference modulation at large displacements for large collection angles. The simulations fail, however, to accurately predict the slight rise in baseline signal as the iris I stopped down. This may reflect a slight misalignment of the optical system or other experimental factors not included in the simulation.

the separation between the bead and the coverslip, λ is the vacuum wavelength of the laser and n is the index of refraction of the medium. This provides a second and much more sensitive method of determining the focal shift. The motion of the stage (d_s) and motion of the focus (d_f) are related through a scaling parameter f_s, which is the fractional focal shift: $d_f = f_s \cdot d_s$. The interference pattern was observed by translating the stage so that the measured spatial frequency was in units of d_s. The spatial frequency then becomes $d_s = \lambda/2 \cdot n \cdot f_s$, which can be rearranged to give f_s, the fractional focal shift parameter: $f_s = \lambda/2 \cdot n \cdot d_s$. The fractional focal shift measured in this manner was 0.799 ± 0.002, which is within the uncertainty of the focal shift as determined from drag-force measurements. The interference method of measuring the focal shift is both easier and more accurate than the method based on drag presented above. Measured values of the focal shift parameter do not agree with numerical results based on the electromagnetic diffraction of a plane-wave focused through an interface (Wiersma et al., 1997). The focal shift was 0.799 ± 0.002 in water with an index of refraction of 1.33, and 0.874 ± 0.004 in a 50% glycerol water mixture, which has an index of refraction of 1.4. The calculated values for these two indices are 0.741 and 0.852 respectively. Whereas this represents only a 7% error at worst, it is well outside the uncertainty in the measurements. This discrepancy may be due to the plane-wave approximation that was made to calculate the focal shifts. Similar experiments in conjunction with calculations based on a Gaussian beam rather than a plane wave approximation may resolve the discrepancy and will allow the testing of theoretical predictions with high precision.

Conclusion

We have demonstrated two-dimensional position detection based on polarization and spatial interferometry in an optical trap. Employing this detection scheme we identified a weak secondary-interference effect due to multiple scattering between the trapped bead and the surface, providing a simple and accurate means of measuring the focal shift. We present a second method of determining the focal shift and a straightforward method for determining the absolute position of the trapped bead with respect to the coverslip. Finally, we have measured the dependence of lateral stiffness on axial position in the optical trap in addition to the ratio of axial and lateral stiffness. The potentially large change in stiffness as a trapped bead is moved in the axial dimension suggests a means to achieve higher forces for a given laser power and bead, but it is also a source of error if it is not appreciated. Measured parameters were compared with theoretical predictions based on electromagnetic calculations and Gaussian beam approximations. With few exceptions the measurements are consistent with the theoretical predictions and with one another. The methods employed are easily adapted to any optical trap and taken together will permit high-resolution determination of both absolute and relative axial motions of trapped particles

References

Allersma, M. W., Gittes, F., deCastro, M. J., Stewart, R. J., and Schmidt, C. F. (1998). Two-dimensional tracking of ncd motility by back focal plane interferometry. Biophys J *74*, 1074-1085.

Ashkin, A. (1970). Acceleration and trapping of particles by radiation pressure. Physical Review Letters *24*, 156-159.

Ashkin, A. (2000). History of optical trapping and manipulation of small-neutral particle, atoms, and molecules. IEEE Journal of Selected Topics in Quantum Electronics *6*, 841-856.

Ashkin, A., Dziedzic, J. M., Bjorkholm, J. E., and Chu, S. (1986). Observation of a Single-Beam Gradient Force Optical Trap for Dielectric Particles. Optics Lett *11*, 288-290.

Clapp, A. R., Ruta, A. G., and Dickinson, R. B. (1999). Three-dimensional optical trapping and evanescent wave light scattering for direct measurement of long range forces between a colloidal particle and a surface. Review of Scientific Instruments *70*, 2627-2636.

Denk, W., and Webb, W. W. (1990). Optical measurement of picometer displacements of transparent microscopic objects. Applied Optics *29*, 2382-2391.

Florin, E. L., Horber, J. K. H., and Stelzer, E. H. K. (1996). High-resolution axial and lateral position sensing using two-photon excitation of fluorophores by a continuous-wave Nd alpha YAG laser. Applied Physics Letters *69*, 446-448.

Florin, E. L., Pralle, A., Horber, J. K. H., and Stelzer, E. H. K. (1997). Photonic force microscope based on optical tweezers and two-photon excitation for biological applications. Journal of Structural Biology *119*, 202-211.

Friese, M. E. J., Truscott, A. G., Rubinsztein-Dunlop, H., and Heckenberg, N. R. (1999). Three-dimensional imaging with optical tweezers. Applied Optics *38*, 6597-6603.

Ghislain, L. P., Switz, N. A., and Webb, W. W. (1994). Measurement of small forces using an optical trap. Rev Sci Instrum *65*, 2762-2768.

Ghislain, L. P., and Webb, W. W. (1993). Scanning-force microscope based on an optical trap. Optics Letters *18*, 1678-1680.

Gittes, F., and Schmidt, C. F. (1998). Interference model for back-focal-plane displacement detection in optical tweezers. Optics Letters *23*, 7-9.

Gosse, C., and Croquette, V. (2002). Magnetic Tweezers: Micromanipulation and Force Measurement at the Molecular Level. Biophys J *82*, 3314-3329.

Greulich, K. O. (1999). Optical trapping and manipulation. In Microsystem technology: a powerful tool for biomolecular studies, H. P. Saluz, ed. (Basel, Switzerland, Birkhauser). Harada, Y., and Asakura, T. (1996). Radiation forces on a dielectric sphere in the Rayleigh scattering regime. Optics Communications *124*, 529-541.

Jonas, A., Zemanek, P., and Florin, E. L. (2001). Single-beam trapping in front of reflective surfaces. Optics Letters *26*, 1466-1468.

Mehta, A. D., Pullen, K. A., and Spudich, J. A. (1998). Single molecule biochemistry using optical tweezers. Febs Letters *430*, 23-27.

Peters, I. M., de Grooth, B. G., Schins, J. M., Figdor, C. G., and Greve, J. (1998). Three dimensional single-particle tracking with nanometer resolution. Review of Scientific Instruments *69*, 2762-2766.

Pralle, A., Prummer, M., Florin, E. L., Stelzer, E. H. K., and Horber, J. K. H. (1999). Three-dimensional high-resolution particle tracking for optical tweezers by forward scattered light. Microscopy Research and Technique *44*, 378-386.

Radler, J., and Sackmann, E. (1992). On the Measurement of Weak Repulsive and Frictional Colloidal Forces by Reflection Interference Contrast Microscopy. Langmuir *8*, 848-853.

Rohrbach, A., and Stelzer, E. H. K. (2002). Three-dimensional position detection of optically trapped dielectric particles. Journal of Applied Physics *91*, 5474-5488.

Sasaki, K., Tsukima, M., and Masuhara, H. (1997). Three-dimensional potential analysis of radiation pressure exerted on a single microparticle. Applied Physics Letters *71*, 37-39.

Stelzer, E. H. K., Florin, E. L., Pralle, A., and Horber, J. K. H. (1998). Photonic force microscope based on optical tweezers and two-photon excitation for biological applications. Abstracts of Papers of the American Chemical Society *216(pt.1)*, 336-COLL.

Svoboda, K., and Block, S. M. (1994a). Biological applications of optical forces. Annu Rev Biophys Biomol Struct *23*, 247-285.

Svoboda, K., and Block, S. M. (1994b). Force and velocity measured for single kinesin molecules. Cell *77*, 773-784.

Videen, G. (1991). Light-Scattering from a Sphere on or near a Surface. Journal of the Optical Society of America a-Optics Image Science and Vision *8*, 483-489.

Videen, G. (1993). Light-Scattering from a Sphere Behind a Surface. Journal of the Optical Society of America a-Optics Image Science and Vision *10*, 110-117.

Visscher, K., and Block, S. M. (1998). Versatile optical traps with feedback control. Methods Enzymol *298*, 460-489.

Visscher, K., Gross, S. P., and Block, S. M. (1996). Construction of multiple-beam optical traps with nanometer-resolution position sensing. IEEE Journal of Selected Topics in Quantum Electronics *2*, 1066-1076.

Wang, M. D., Yin, H., Landick, R., Gelles, J., and Block, S. M. (1997). Stretching DNA with optical tweezers. Biophys J *72*, 1335-1346.

Wiersma, S. H., Torok, P., Visser, T. D., and Varga, P. (1997). Comparison of different theories for focusing through a plane interface. Journal of the Optical Society of America á-Optics Image Science and Vision *14*, 1482-1490.

Wright, W. H., Sonek, G. J., Tadir, Y., and Berns, M. W. (1990). Laser Trapping in Cell Biology. IEEE J Quantum Electronics *26*, 2148-2157.

Zhang, Z. X., Sonek, G. J., Liang, H., Berns, M. W., and Tromberg, B. J. (1998). Multiphoton fluorescence excitation in continuous-wave infrared optical traps. Applied Optics *37*, 2766-2773.

Chapter 3

Abstract

RNA polymerase (RNAP) translocates along a DNA template with variable rates and frequent pauses. To investigate the mechanisms of transcription, we have determined the effect of hindering and assisting forces on the transcriptional velocity and pausing of single *E. coli* RNAP molecules, using an optical trap that allows the detection of pauses as short as one second. Although our naturally transcribed template lacks known regulatory pauses, we detected a class of short pauses that are not the result of RNAP backtracking along the template. Additionally, we observe a population velocity distribution that implies multiple velocity states, although individual molecules appear to move with a single velocity. We find no evidence of switching between velocity states.

Introduction

During transcription, the motion of RNA polymerase (RNAP) is discontinuous. The rate of translocation is variable and often decreases to zero during transcriptional pauses (Kassavetis and Chamberlin, 1981; Levin and Chamberlin, 1987; Lyakhov et al., 1998; Matsuzaki et al., 1994; Reisbig and Hearst, 1981). Some pauses serve to regulate gene expression (reviewed in: (Chan and Landick, 1994; Landick and Yanofsky, 1987; Richardson and Greenblatt, 1996; Uptain and Chamberlin, 1997; Uptain et al., 1997), whereas the majority of observed pauses are thought to simply limit the average rate of transcription. Several long-duration, high-efficiency regulatory pauses have been characterized (Artsimovitch and Landick, 1998; Artsimovitch and Landick, 2000; Chan and Landick, 1989; Landick, 1997; Landick et al., 1987; Landick et al., 1996; Mooney et al., 1998; Palangat and Landick, 2001; Yin et al., 1999). Short-duration, low-efficiency

pauses, however, are not amenable to study by means of conventional biochemical approaches and consequently, are poorly characterized. When global transcriptional pausing has been investigated on a given template, pausing was found to be ubiquitous. Pauses occurred within, as well as between, genes in a polysistronic template, and pause lifetime and efficiency were heterogeneous (Kassavetis and Chamberlin, 1981; Matsuzaki et al., 1994). While the observed pauses clearly depend on the template sequence and nucleotide concentration, the origin of these pauses remains unclear.

Nudler and coworkers have introduced a model of transcription that suggests a mechanical origin for these ubiquitous transient pauses (Komissarova and Kashlev, 1997a; Landick, 1997; Nudler, 1999; Nudler et al., 1997). In the sliding clamp model of transcription, the polymerase can backtrack along the DNA template while maintaining the RNA-DNA hetero-duplex. This forces the 3' end of the nascent RNA out of the nucleotide pore and occludes the active site, which in turn blocks transcription and induces a pause. A short, one or more nucleotide, backtracking event that can be thermally relieved, induces a transient pause. Larger backtracking motions result in longer pauses or transcriptional arrest. While there is evidence for the long-lived and arrested backtracked states (Komissarova and Kashlev, 1997b; Palangat and Landick, 2001; Reeder and Hawley, 1996; Toulme et al., 1999), the origin of the short pauses remains untested. A related model has been proposed to describe the force-velocity relationship for RNAP in which the decrease of velocity at high hindering loads results from increased pausing (Wang et al., 1998). Both models make testable predictions with respect to the relationship between force, transcriptional pausing, and velocity.

Transcriptional pausing is also implicated in both the heterogeneity of transcription rates measured *in vitro* and the differences between mean rates measured *in vivo* and *in vitro*. Kassavetis and Chamberlin have suggested that the two- to five-fold difference between *in vivo* and *in vitro* transcription rates reflects the relief of pausing *in vivo*, possibly through the interaction of RNAP with an unknown protein cofactor (Kassavetis and Chamberlin, 1981). Large differences in transcription rates of identical RNAP molecules transcribing the same template have been observed in both bulk assays and in single-molecule experiments (Davenport et al., 2000; Kassavetis and Chamberlin, 1981; Matsuzaki et al., 1994; Reisbig and Hearst, 1981; Yin et al., 1994; Yin et al., 1995). Velocity heterogeneity has been attributed to pausing (Kassavetis and Chamberlin, 1981), as well as the ability of RNAP molecules to switch between two different velocity states during transcription (Matsuzaki et al., 1994). A recent single-molecule study of *E. coli* RNAP provides evidence for two velocity states between which individual molecules switch on a slowtime scale (Davenport et al., 2000). The limited temporal resolution of this experiment, however, makes it difficult to unambiguously separate pauses from translocation, permitting alternative interpretations (Guthold and Erie, 2001).

To test models of transcriptional pausing and to investigate the interplay between pausing and velocity, we developed a feedback-enhanced optical trap that can record the motion of single *E. coli* RNAP molecules transcribing under constant assisting or hindering loads with high temporal bandwidth. The assay was further improved by means of a specific biotin linkage of the RNAP molecules to their supports, as opposed to the non-specific

adsorption previously employed (Wang et al., 1998; Wang et al., 1997; Yin et al., 1995). These improvements provide significant advantages over previous single-molecule studies of RNAP. Specifically linking RNAP molecules to optically trapped beads created a reproducible geometry, which eliminated the uncertainty in the direction of applied load previously encountered in assays with a fixed support (Wang et al., 1998; Yin et al., 1995). High-bandwidth position detection in 2 dimensions was achieved through the combination of interferometric optical detection and a calibrated, position-stabilized, three-axis, piezoelectric stage. Previous optical trapping studies of RNAP relied on approximations and calculated corrections for the effects of motion in the axial direction (Wang et al., 1998; Wang et al., 1997; Yin et al., 1995), whereas in this study these corrections were either directly measured or were included in the initial calibrations. Moreover, incorporation of the piezoelectric stage into a force-feedback loop permitted recording motion over thousands of base pairs (bp) at a constant force with an aggregate data rate of 50 Hz. Previous studies have suffered from either a continuously changing force (Wang et al., 1998) or a data rate and resolution limited by video acquisition (Davenport et al., 2000). Complementing these technical improvements, the ability to apply both hindering and assisting loads enabled investigation of the effects of force over a nearly 70-pN range, thereby making it possible to elucidate weak and subtle effects of applied load on transcription, and to extend the force-velocity relationship of *E. coli* RNAP into the regime of assisting forces. The advantages of single molecule measurements have been well documented (Mehta et al., 1999; Moerner and Orrit, 1999; Weiss, 1999). For RNAP in particular, single molecule measurements permit detection of low probability and short duration events inaccessible

to conventional biochemical assays. Employing this assay we have determined the effect of force on pausing, providing a test of the sliding clamp model for transient pauses as well as certain force-velocity models. Additionally, the ability to measure transcription over many kilo-bases, coupled with the ability to distinguish transient pauses from motion, has allowed us to investigate the origin of the velocity distribution.

Results and Discussion

Assay

Implementation of the single molecule trapping assay is illustrated in Fig. 3.1A. In the assay, a stalled ternary complex consisting of a DNA template that comprises a portion of the *rpoB* gene of *E. coli*, nascent RNA and a single biotin-labeled RNAP molecule was attached to an avidin-coated polystyrene sphere 500 nm in diameter. This complex was tethered to the surface of a flow cell via a digoxigenin antibody located on the upstream end (for assisting loads) or downstream end (for hindering loads) of the DNA. Addition of nucleotide triphosphates (NTPs) restarted transcription. The bead was trapped, the attachment point of the tether was determined (Wang et al., 1998; Wang et al., 1997; Yin et al., 1995), and the bead was moved to a predetermined position in the optical trap. The bead was held fixed in the optical trap by moving the stage to compensate for the motion of the polymerase along the DNA. This maintained a constant force on the bead, since the optical trap applies a force proportional to the displacement of the bead from the

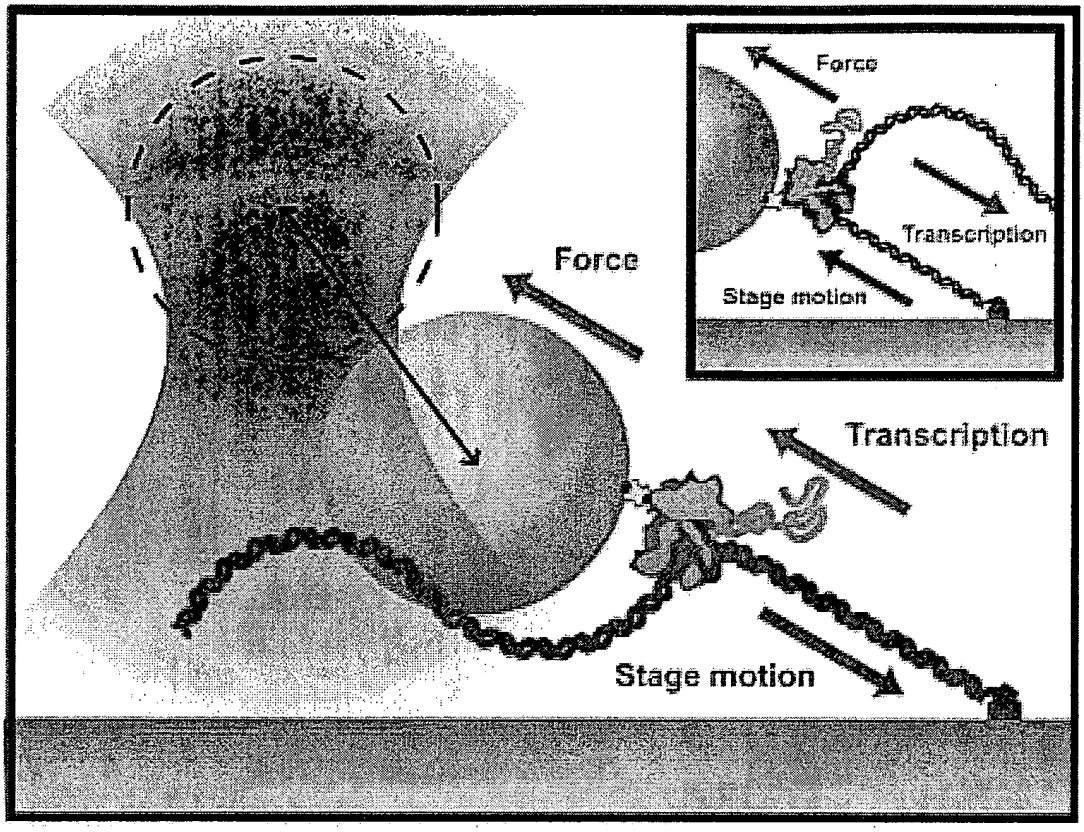

Figure 3.1 A. Cartoon of experimental geometry (not to scale). The transcribing RNA polymerase (green, nascent RNA in gold) is specifically attached to a polystyrene bead (blue) via a biotin-avidin linkage (yellow). The upstream end of the DNA (red and blue) is attached through a digoxigenin-antidigoxigenin pair (purple) to the surface of the flow cell (blue), which is affixed to a feedback-controlled piezoelectric stage. The bead is held in the optical trap (pink) at a predetermined distance (black arrow) from the equilibrium position (dotted circle), which results in restoring force exerted on the bead (pink arrow). During transcription (green arrow), the position of the bead in the optical trap and hence the applied force, is held constant by moving the stage to compensate for the motion of the polymerase along the template (blue arrow). For the geometry depicted in the cartoon, the applied force is in the direction of transcription (assisting load). By placing

the digoxigenin label on the downstream end of the DNA, the direction of transcription with respect to the optical trap is reversed and the applied load opposes transcription (hindering load) (inset).

equilibrium position of the trap. The motion of the polymerase was derived from the motion of the stage corrected for the elastic compliance of the DNA (Wang et al., 1998; Wang et al., 1997). As seen in a representative trace (Fig. 3.1B), the motion of the polymerase was frequently interrupted by pauses of variable duration. To quantify the pausing behavior and measure the velocity of single RNAP molecules, individual traces were smoothed with a second-order Savitzky-Golay filter over a 2.5 second window and differentiated to obtain the instantaneous velocity (Fig. 3.1B lower panel). The velocity distribution (Fig. 3.1B left inset) was invariably bimodal, and accordingly, the distribution was fit with a sum of two Gaussians. The peak near 0 bp/s corresponds to pausing, whereas the second peak reflects the average transcription rate. Pauses were scored when the velocity dropped below half the Gaussian peak velocity (Fig. 3.1B). Simulations showed that this method reliably detected pauses as short as 1 s (data not shown). The data presented was obtained from a set of 143 traces such as that shown in Fig. 3.1B, except for the force-velocity relationship data, which shares the same experimental geometry (Fig. 3.1A) but was obtained with a different optical trapping protocol.

Force-velocity relationship

(Translocation step is not rate limiting at low load)

The force-velocity (F-V) relationship for individual RNAP molecules is presented in Fig. 3.2. The optical trap, in position clamp mode (Wang et al., 1998; Wang et al., 1997), was used to record the hindering (positive) force portion of the curve, whereas a linear force-ramp mode was used to collect the assisting (negative) force data (see Materials

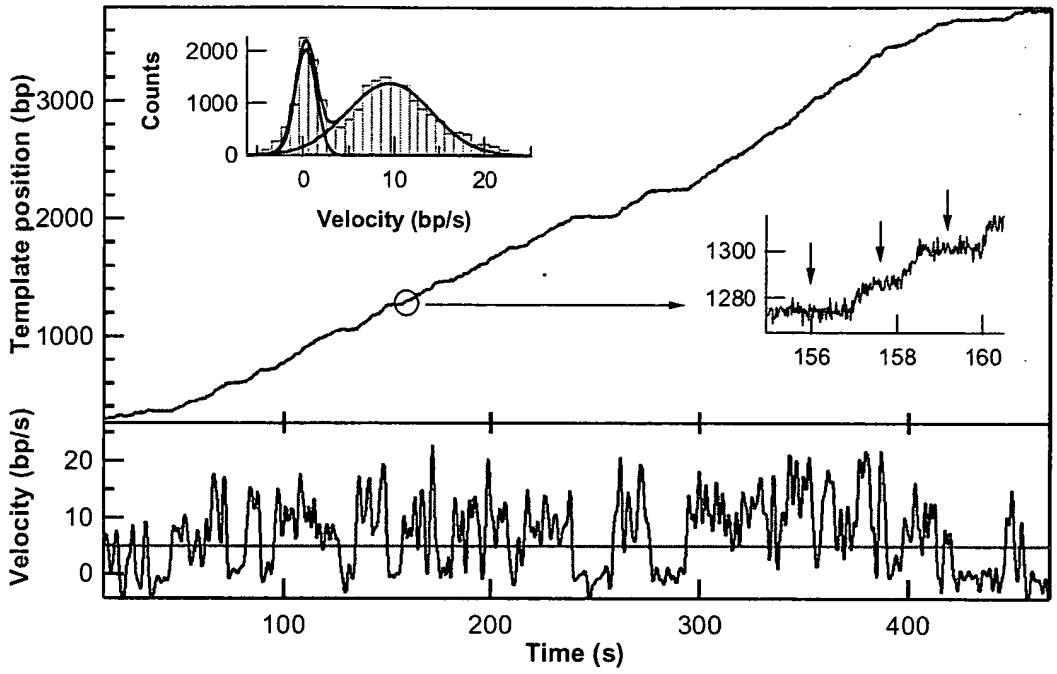

Figure 3.1 B. RNA polymerase translocation and pausing under load. Representative record of elongation for a single polymerase molecule transcribing 3.5 kb of DNA (1 mM NTPs) under 18 pN of hindering load (red trace) and the instantaneous elongation velocity (blue trace). Pauses of several seconds can readily be seen in the position and velocity traces while pauses as short as one second can be discerned in the expanded section of the trace (right inset, arrows indicate position of pauses). The velocity histogram (left inset) is bimodial with a peak centered near zero corresponding to pauses and a peak at 9.5 bp/s corresponding to the average rate of transcription. Data were obtained by sampling the position of the bead at 2 kHz and averaging over 40 points to generate a 50 Hz feedback signal that controlled the stage. The motion of the polymerase along the DNA template was obtained from the trajectory of the stage corrected for the

elasticity of the DNA. The corrected traces were smoothed with a 2nd order Savitzky-Golay filter (τ = 2.5 s) and differentiated to obtain the instantaneous velocity. The velocity distribution (left inset) is fit with a Gaussian and pauses are scored when the velocity falls below half the Gaussian center velocity (gray line on the velocity trace).

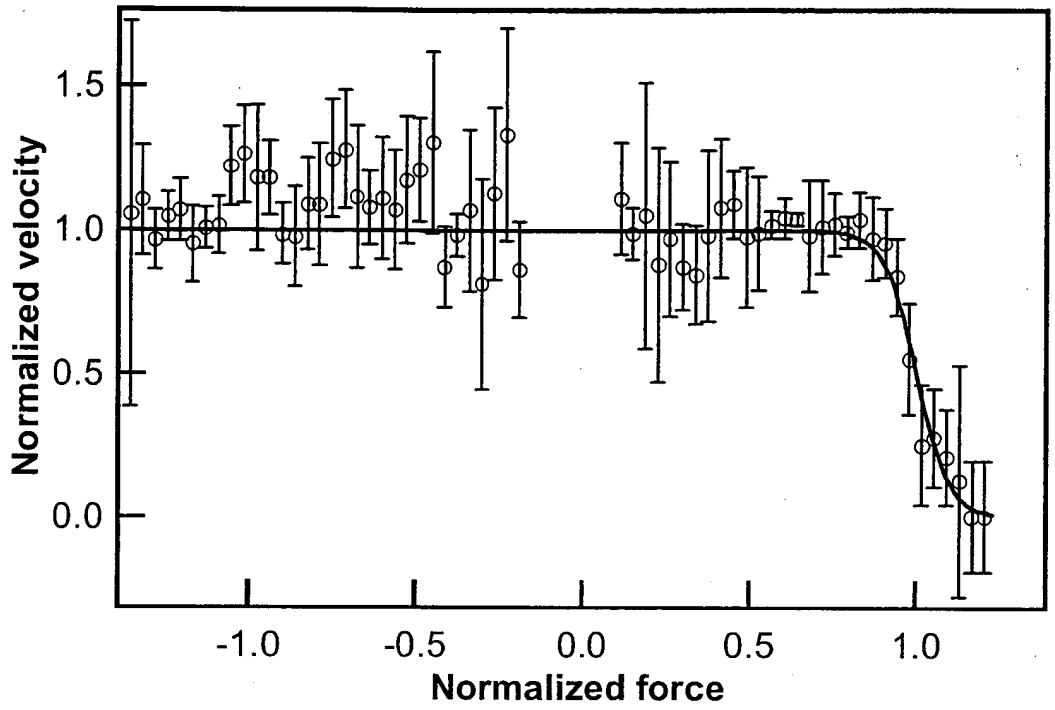

Figure 3.2. Force-velocity relationship for RNA polymerase. Normalized velocity (mean ± s.d.) versus normalized force at 1 mM NTP fit to *f-v* model (line). Fit parameters: a = $7.4 \pm 4.1 \times 10^8$; $\langle F_{1/2} \rangle = 27 \pm 2$ pN, corresponding to a δ of 9 ± 1 bp. The positive (hindering) force regime is an ensemble average of 21 individual normalized *F-V* traces derived from position clamp records. The negative (assisting) force regime is an ensemble average of 13 individual normalized *F-V* traces obtained from increasing force records and normalized to the $F_{1/2}$ from the positive force *F-V* trace. The good agreement between the data and the fit near stall is probably an artifact of averaging over many records with different stall forces. Individual traces typically enter stall abruptly and do not display the slight curvature seen in the fit and the last few points of the average data.

and Methods). In the position-clamp mode, the RNAP molecule was prevented from moving by increasing the force applied to the bead. As the force increased, the enzyme slowed down before stalling, thereby providing the F-V relationship for a single enzyme. The position clamp cannot measure the single-molecule F-V relationship for an assisting force. Therefore, a routine was implemented allowing measurement of this portion of the F-V curve by linearly increasing the force on the bead during transcription. Traces obtained under hindering forces were normalized by the low load velocity (V_0) and by the force at which the velocity decreased to half the maximal value ($F_{1/2}$) and averaged together (Wang et al., 1998). This normalization scheme permitted combining F-V curves for enzymes with different maximal velocities and stall forces. Traces obtained under assisting loads were normalized by the low load velocity and by the average $F_{1/2}$ obtained from the hindering-load traces. The resulting F-V curve is well fit by an equation of the form

$$V(F) = \frac{V_0(1+A)}{1+A\exp(F\delta/k_BT)} \quad (3.1)$$

where V_0 is the unloaded velocity, δ is a characteristic distance through which the applied load acts, and A is a dimensionless constant that describes the degree to which mechanical or biochemical steps limit the motion in the absence of load. A is << 1 if biochemical steps limit the rate whereas A >1 if mechanical steps are limiting. Once the data have been normalized, the equation reduces to a much simpler form (Wang et al., 1998).

$$v(f) \approx \frac{1}{1+a^{f-1}} \quad (3.2)$$

where

$f = F/F_{1/2}$
$v = V/V_0$
$a = \exp(F_{1/2}\delta/k_BT)$

The normalized *f*-v relation is described by a single free parameter, *a*, which can be combined with the average $F_{½}$ to obtain δ. The measured *f*-*v* curve was fit with an *a* parameter of $7.4 \pm 4.1 \times 10^8$. The average $F_{1/2}$ was 27 ± 2 pN Corresponding to a δ of 9 ± 1 bp, which is in good agreement with δ in the range of 7.0-8.7 bp previously reported (Wang et al., 1998).

The flatness of the F-V curve for all assisting loads and hindering loads approaching stall supports the previous conclusion that translocation is not the rate-determining step at low loads (Wang et al., 1998). Extending the F-V curve to the regime of assisting loads provides a more stringent test of this hypothesis, which is born out by the degree to which the model (Equation 3.1) fits the data (Fig. 3.2). Furthermore, the asymmetry in the F-V relation lends support to the assertion that the decrease in velocity at high loads results from the challenge of a mechanical transition in the translocation cycle, rather than a perturbation of the protein structure due to the applied load. If the decrease in velocity were due to a load-induced structural change then velocity should also be affected by high assisting loads, which is not the case. In the previous study, the variance in the $F_{½}$

value for different RNAP molecules was potentially due to the uncertainty in the direction of the applied load (Wang et al., 1998). Improved trapping geometry and specific attachment of the RNAP ought to alleviate this uncertainty, yet the variance in $F_{½}$ between enzymes in this study is similar to the previous study. This suggests that the differences in stall forces and $F_{½}$ forces are a result of sequence dependent effects or to differences between the enzymes themselves.

Velocity Distribution

(Transcription rate for individual enzymes is constant but population distribution is broad)

The velocity distributions for individual RNAP molecules (Fig. 3.3A) share common features. Each distribution has a peak near zero that corresponds to pausing and a broader peak at a positive velocity that represents transcription. Analysis of the data sets failed to reveal evidence for a third peak, i.e., a second distinct velocity state. Each peak was individually well fit by a Gaussian and the entire distribution for each data set was fit by the sum of two Gaussians. The width of the pause distribution is indicative of the noise in the system. The velocity distribution was broader than the pause distribution as a consequence of the stochastic nature of the motion. An enzyme moving stochastically at a constant average rate displays a velocity distribution centered on the average rate, with a width inversely proportional to the number of rate-determining steps. The observed velocity distribution is a convolution of the noise distribution and the intrinsic velocity distribution of the enzyme due simply to the random nature of translocation. The combined effects of positional uncertainty, smoothing and experimental factors that

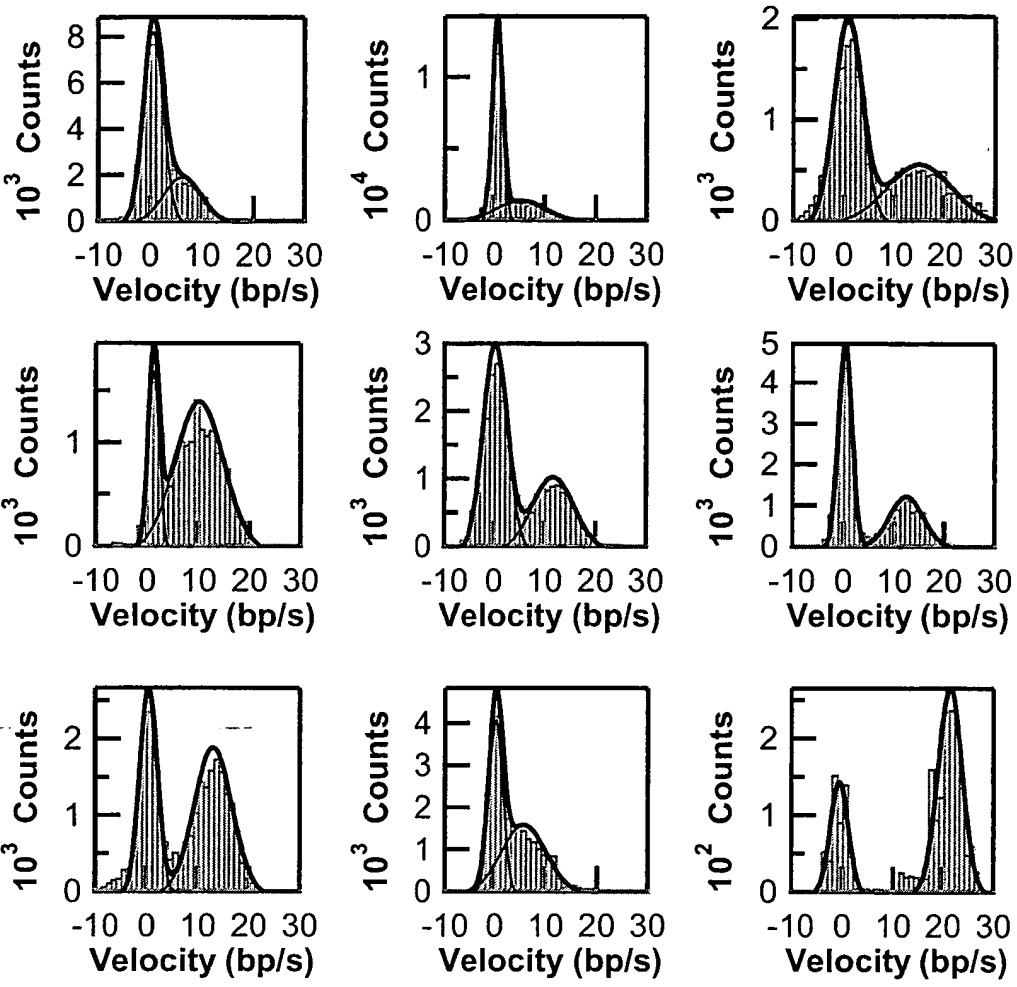

Figure 3.3 A. Velocity distributions for individual traces. Histograms of instantaneous velocity for 9 runs at 1mM NTPs fit to the sum of two Gaussian distributions (heavy line, light lines correspond to the individual Gaussians). The peak near 0 bp/s corresponds to pausing whereas the second peak corresponds to transcription. (i) 25 pN, (ii) 19 pN, (iii) 14 pN, (iv) 9 pN , (v) -8 pN (vi) -15 pN (vii) -17 pN (viii) -33 pN (ix) -33 pN.

influence the width of the velocity distribution make direct calculation of the expected velocity distributions difficult. Comparisons between measured and simulated transcription records suggest that the velocity distributions are consistent with a single, invariant, rate-determining step for translocation (data not shown). Whereas individual RNAP molecules appear to transcribe at a single rate, these rates vary across the population of molecules (Fig. 3.3 B). A parameter-free variance test was applied to the run-velocity distributions to determine if the motion of individual RNAP molecules could be described by a single broad distribution. Results of the Kruskal-Wallis or H-test do not support a single velocity distribution ($p>99.9$). Thus, the observed population variance reflects multiple underlying velocity states rather than a single state with a broad distribution.

The average peak fit velocity was 9.7 ± 0.4 bp/s (mean ± s.e.m. n=143) for 1 mM NTPs. This is comparable to velocities reported for *E. coli* RNAP, which range from 10 to 16 bp/s in single molecule studies (Wang et al., 1998; Yin et al., 1994), and 13 to 20 bp/s for solution studies under similar conditions (Schafer et al., 1991). The average velocity including pauses was 6.2 ± 0.4 bp/s, which is comparable to previously measured single molecule rates of 8.0 ± 3.0 bp/s (Davenport et al., 2000). The translocation rate was independent of template position and applied force over the range investigated (data not shown), consistent with previous measurements (Davenport et al., 2000).

Despite the ability to distinguish short pauses from translocation, the measured peak velocities are still several-fold lower than transcription velocities reported *in vivo*.

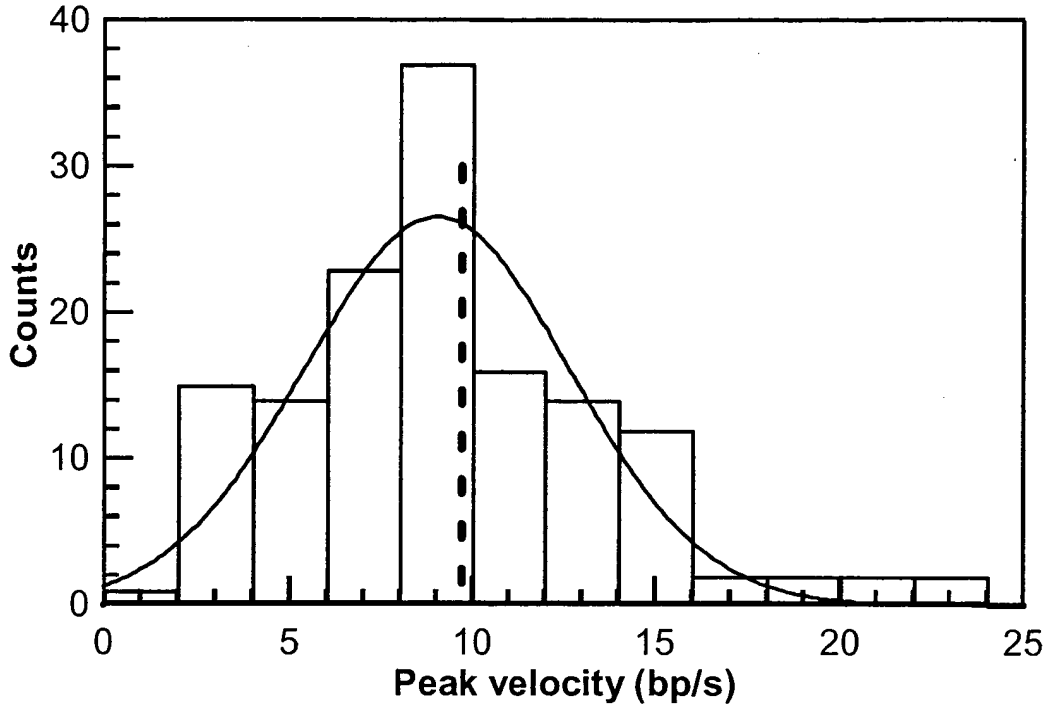

Figure 3.3 B. Velocity distribution. Histogram of Gaussian peak-fit velocities from 143 runs. The histogram is fit with a Gaussian distribution centered at 9.0 bp/s with a width of 3.65 bp/s ($\chi_\omega^2 = 1.75$). The average velocity (dashed line) is 9.7 ± 0.4 bp/s (mean ± s.e.m. n=143) with a standard deviation of 5.0 bp/s.

Correcting the measured velocities for the effects of the pauses that were too short to detect results in only a slight increase in translocation rate (11.3 bp/s). Pausing on the time scale of a second and longer, therefore, is not sufficient to explain the discrepancy between *in vivo* and *in vitro* transcription rates. The data do not, however, exclude the possibility of a very short, high probability pause that could act to limit transcription *in vitro*. Using a similar approach, it was verified that the population velocity distribution represented different intrinsic translocation rates rather than different propensities to pause. The distribution of corrected velocities was similar to the uncorrected (data not shown), implying that multiple velocity states, rather than multiple pause prone states govern the distribution of measured transcription rates.

Pause lifetime distribution

(Two or more transcriptional pause lifetimes)

High bandwidth recording of single RNAP molecules coupled with automated pause detection permitted a kinetic analysis of pauses that is difficult or impossible to achieve with conventional bulk transcription assays visualized on polyacrylimide gels (Kassavetis and Chamberlin, 1981; Landick et al., 1996; Matsuzaki et al., 1994). Constraints and assumptions needed to derive kinetic parameters from such assays are significantly relaxed when individual molecules are considered. Moreover, short, low-probability pauses, undetectable through gel analysis, are readily detected in single-molecule experiments. For all 143 force-clamp records, pauses were scored and the applied force, position and duration of each pause were recorded. Initially, pauses were pooled to

obtain the average behavior. The distribution of pause lifetimes (Fig. 3.4) was well described by a double exponential (p >99%), consistent with at least two pause lifetimes; 60% of pauses had a lifetime of 1 s and 40% had a lifetime of 5.6 s. There are almost certainly additional pause lifetimes as the pause distribution has a very long, low probability tail that was not included in the fit due to the limited number of points. Pauses up to 400 s were observed, however the vast majority of pauses are well described by the double exponential fit. Multiple transcriptional pause lifetimes are observed in long templates (Kassavetis and Chamberlin, 1981; Levin and Chamberlin, 1987; Matsuzaki et al., 1994) and would be expected in any mechanism that included sequence-dependent pausing. Alternatively, different lifetimes could arise from diverse pause mechanisms. To investigate this possibility, pauses were divided into two groups based on their duration. A threshold time of 2.6 s, which corresponds to the duration at which both pause populations are equally probable, was chosen to separate the pauses into long and short categories for further analysis.

Pause probability distribution

(Transcriptional pausing is ubiquitous)

The sequence dependence of transcriptional pauses can shed light on the origin of pausing. Pauses have been attributed to the formation of secondary structure in the nascent RNA (Chan and Landick, 1994; Mooney et al., 1998; Uptain et al., 1997) and to regions of weak DNA-RNA hybrid strength (Artsimovitch and Landick, 2000; Nudler, 1999; Palangat and Landick, 2001). Not all pauses, however, can be explained by either of these mechanisms. The absolute spatial accuracy of the optical trapping records is

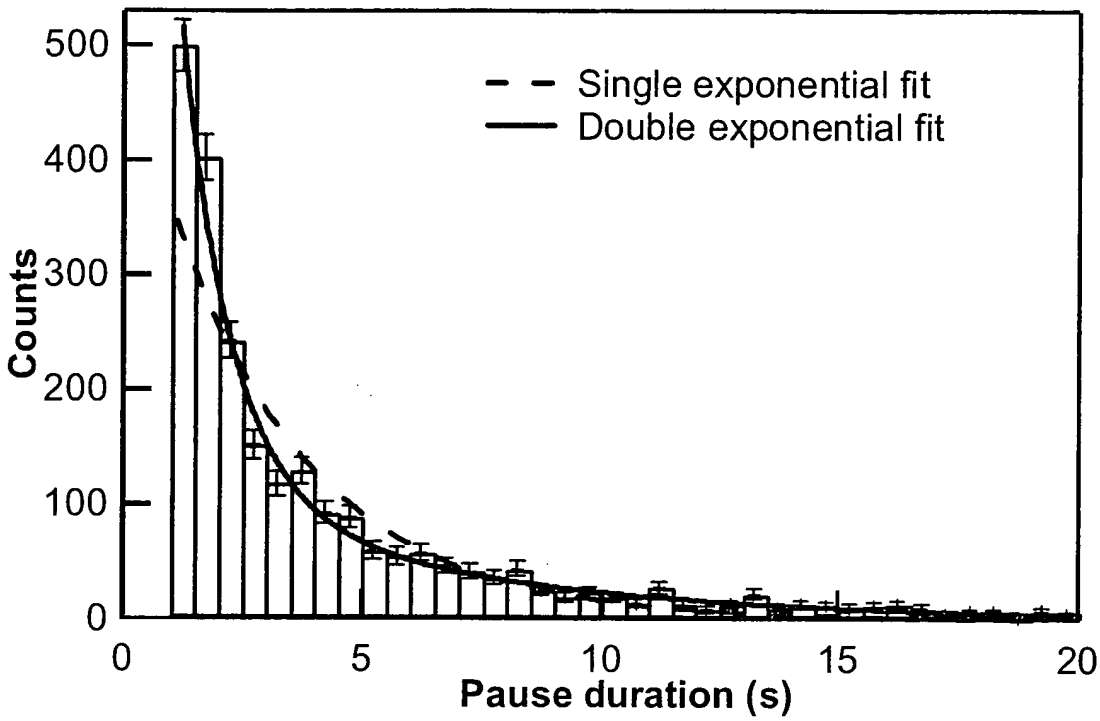

Figure 3.4. Distribution of pause durations measured from pooled data. Pauses shorter than 1 second are excluded from the analysis. The graph is cut off at 20 seconds for clarity. Data are displayed as $N \pm \sqrt{N}$. The pause distribution is well fit by a double exponential (Solid line) ($A_1 = 1100 \pm 100$, $\tau_1 = 1.0 \pm 0.2$ s. $A_2 = 130 \pm 20$, $\tau_2 = 5.6 \pm 0.4$ s. $\chi^2_\upsilon = 1.8$) while only poorly fit by a single exponential (dashed line) ($\chi^2_\upsilon = 7.1$). An F_{test} analysis shows that the double exponential fit is greater than 99% more likely than the single exponential fit. The pause duration distribution has a very long, low probability tail that is not fit by the double exponential distribution (pauses as long as 400 seconds were observed). However, as there are so few events, it is impossible to fit this long tail with any certainty.

limited to ~100 bp, therefore calculating the pause probability density over 100 bp bins is more appropriate than the pause probability at every template position. These uncertainties also preclude measuring pause characteristics for a given pause across different RNAP molecules, only average pause parameters can be measured for each enzyme. Fig. 3.5 illustrates the pause probability density versus template position for all pauses (Fig. 3.5, panel A), long pauses (Fig. 3.5, panel B) and short pauses (Fig. 3.5, panel C). The pause probability density varies only slightly over the entire template in all three cases, suggesting that pausing is either only weakly dependent on sequence or induced by a commonly occurring sequence or sequences. The similarity of the long and short pause probability density histograms is also consistent with multiple origins. The long and short duration pauses could represent different decay rates from a common origin, or they could have distinct origins that are almost equally as common throughout the template. The pause probability density for long and short pauses does not depend significantly on the exact choice of threshold lifetime. The relative probabilities change, but the overall lack of sequence dependence remains until very long or very short threshold times are used, at which point statistical uncertainties dominate the results (data not shown). The flat probability distribution may reflect averaging of pauses that arises from the uncertainty in the position measurements. In an attempt to correct for this, pause positions from individual traces were correlated with one another (data not shown). The lack of any significant correlation between traces suggests that pausing at any given template position is rare, i.e. the probability of pausing is always low. The average pause probability density was 0.0087 bp^{-1}, which underestimates the actual pause probability because short pauses were not detected. The measured pause lifetime distribution

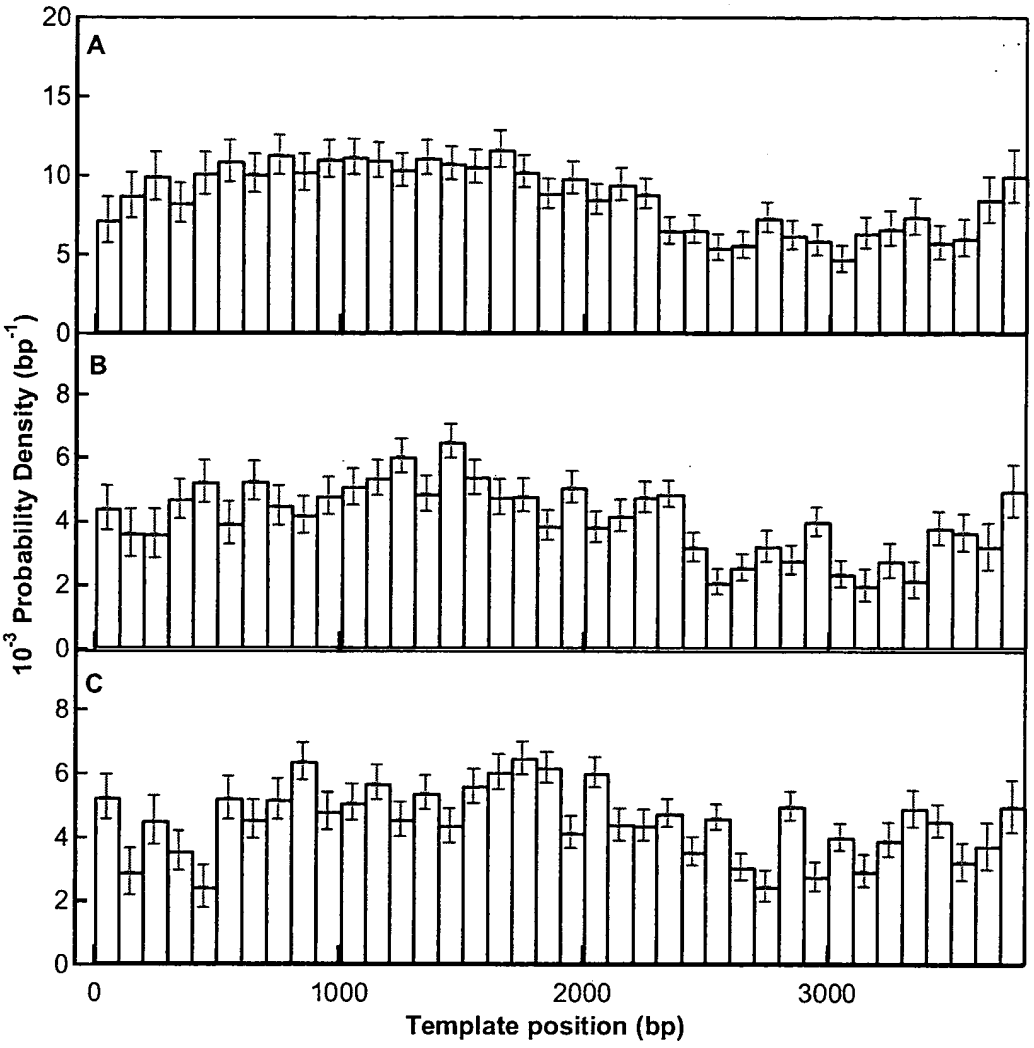

Figure 3.5. Pause probability density for pooled data. The template was divided into bins of 100 bp and the average pause probability density in each bin was calculated by dividing the total number of pauses by the number of records in the bin. The data are represented as mean ± s.d. A. Pause probability density for all pauses. (Average = 0.0087 ± 0.0003 bp^{-1}). B. Pause probability density for long pauses (≥2.6 s; Average = 0.0041 ± 0.0002 bp^{-1}). C. Pause probability for short pauses (<2.6 s; Average = 0.0045 ± 0.0002 bp^{-1}).

(Fig. 3.4) can be used to correct for the missing pauses, which results in an average pause probability density of 0.016 bp^{-1}. As this is an average quantity, it could represent infrequent, high-probability pauses or frequent, low-probability pauses. Given the flat pause probability density distribution and lack of strong correlation in pause location between traces, we favor the second scenario, though it is impossible to quantify the exact frequency and probability of pausing from the current data.

Force dependence of pausing

(Pausing is unaffected by force)

The sliding clamp model of transcription (Nudler, 1999) proposes that transient pausing is the result of reversible backtracking of the polymerase along the DNA template by one or more base pairs. A similar model was proposed as a possible explanation of the force-velocity relationship of RNAP (Fig. 3.2), in which the decrease in velocity at high loads is due to an increase in pause probability and lifetime (Wang et al., 1998). The backsliding model predicts a similar increase in pausing with hindering loads and a reduction of pausing with assisting loads. The force dependence of backtracking can be understood by appealing to Fig. 3.6A, which casts the backtracking model in an energy landscape representation with distance as the reaction coordinate. A single energy barrier separates paused and elongation competent states that are a distance δ_{total} apart and a distance δ_2 and δ_1 from the barrier, respectively. The application of load changes the free energy of the pause and elongating states relative to the transition state. The rate of pausing, k_p and the rate of returning to the elongating pathway, k_{-p} are modified by an Arrhenius factor giving:

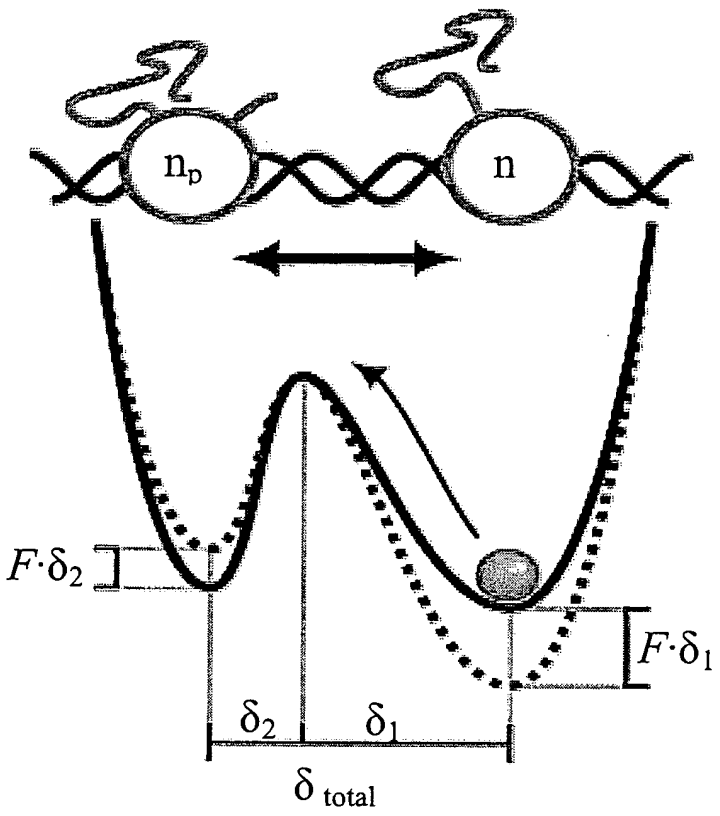

Figure 3.6 A. Cartoon depicting the RNAP backtracking model of pausing and associated schematic free energy diagram. The backtracking model proposes that transient pauses (state n_p) during transcription (state n) arise from the RNAP (green circle) sliding backwards along the template DNA (red and blue) by one or more bases (distance δ_{total}) while maintaining the RNA-DNA hetero-duplex. The resulting motion of the 3' end of the nascent RNA (gold) relative to the polymerase occludes the active site and prevents further transcription until the motion is reversed (returning to state n). The corresponding free energy diagram is a single barrier between two potential wells separated by a distance δ_{total}. The barrier is a distance δ_1 from the initial well, the normal elongation state (state n). The application of an external load alters the potentials by the amount indicated (Dotted line, initial; solid line, final).

$$k_p = k_p^0 \exp(F \cdot \delta_1 / k_B T) \qquad (3.3)$$

and

$$k_{-p} = k_{-p}^0 \exp(-F \cdot \delta_2 / k_B T) \qquad (3.4)$$

where k^0 is rate in the absence of load. A similar line of reasoning leads to the expression for the F-V relation (equation 3.1) (Wang et al., 1998). The exponential dependence of pausing parameters on force presents an easily testable prediction of the backsliding model. To test this prediction, the average pause lifetime (k_{-p}^{-1}) and the average pause density (pauses/bp) for both long and short pauses were calculated as a function of force (Fig. 3.6B). Pause density was chosen as a measure of the propensity to pause because it is insensitive to the forward rate of the enzyme. There is evidence from this and other studies (data not shown and Davenport et al., 2000) that pausing is in kinetic competition with translocation, hence slower enzymes tend to pause more frequently. To eliminate this potential artifact, the pause rate is normalized by the translocation rate to obtain the pause density. In practice, this has the effect of changing the pre-factor in the expression for k_p without changing the force dependence. Pause density and lifetime of both long and short pause populations are largely unaffected by hindering or assisting loads from ~25 to ~-40 pN (Fig. 3.6B). While these results are qualitatively inconsistent with the backtracking model of pausing, they do not allow a direct quantitative comparison with the model because of the uncertain location of the transition state with respect to the pause and translocation states. In the backtracking model the distance between the pause

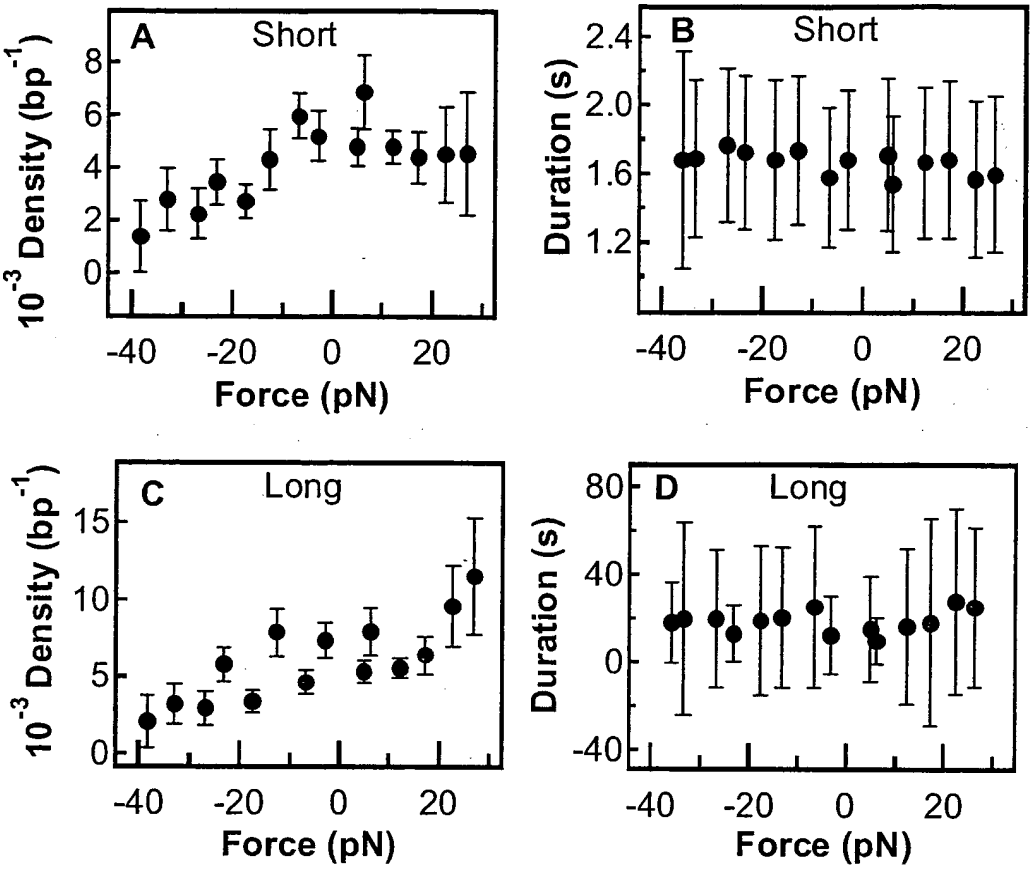

Figure 3.6B. Force dependence of pause duration and pause density. Pauses from individual runs were pooled and binned according to the force at which the pause occurred (5 pN bins). The distance transcribed for each force bin was calculated and used to generate the pause density. The pause density and average pause duration (mean ± s.d.) in each bin are plotted against the average force for that bin. A. Short pause density. B. Short pause duration C. Long pause density D. Long pause duration.

and translocation states is defined as one or more bp but the position of the transition state is undefined. The product of the pause density and pause lifetime, which we refer to as pause strength (P.S.), is proportional to the ratio of k_p and k_{-p}:

$$P.S. \propto \exp(F \cdot (\delta_1 + \delta_2)/k_B T)$$
$$= \exp(F \cdot \delta_{total}/k_B T) \qquad (3.5)$$

Pause strength, thus depends on the total distance between the pause and translocation states and allows a direct comparison with predictions of the backtracking model of pausing. Pause strength as a function of applied load for long and short pauses is displayed in Fig. 3.7. Measured pause strength does not compare well with the predicted curve for a single bp backtracking event (dashed curves in Fig. 3.7). Longer backtracking distances would increase the exponential dependence on force, resulting in steeper curves that deviate further from the measured pause strength. Similarly, symmetric sliding models in which the polymerase can enter a pause by sliding backwards or forwards along the template would result in a curve that is a reflection about the origin of the positive force portion of the expected curve. Exponential fits to pause strength (solid lines in Fig. 3.7) return distances for both long and short pauses that are a fraction of a bp, and are within uncertainty of one another (Fig. 3.7 legend). These results do not depend critically on the choice of threshold time between long and short pauses. As the threshold time is changed, the long and short pause curves change slightly but they remain independent of force (data not shown). These results are inconsistent with the backtracking model of pausing, suggesting that the observed pauses have a

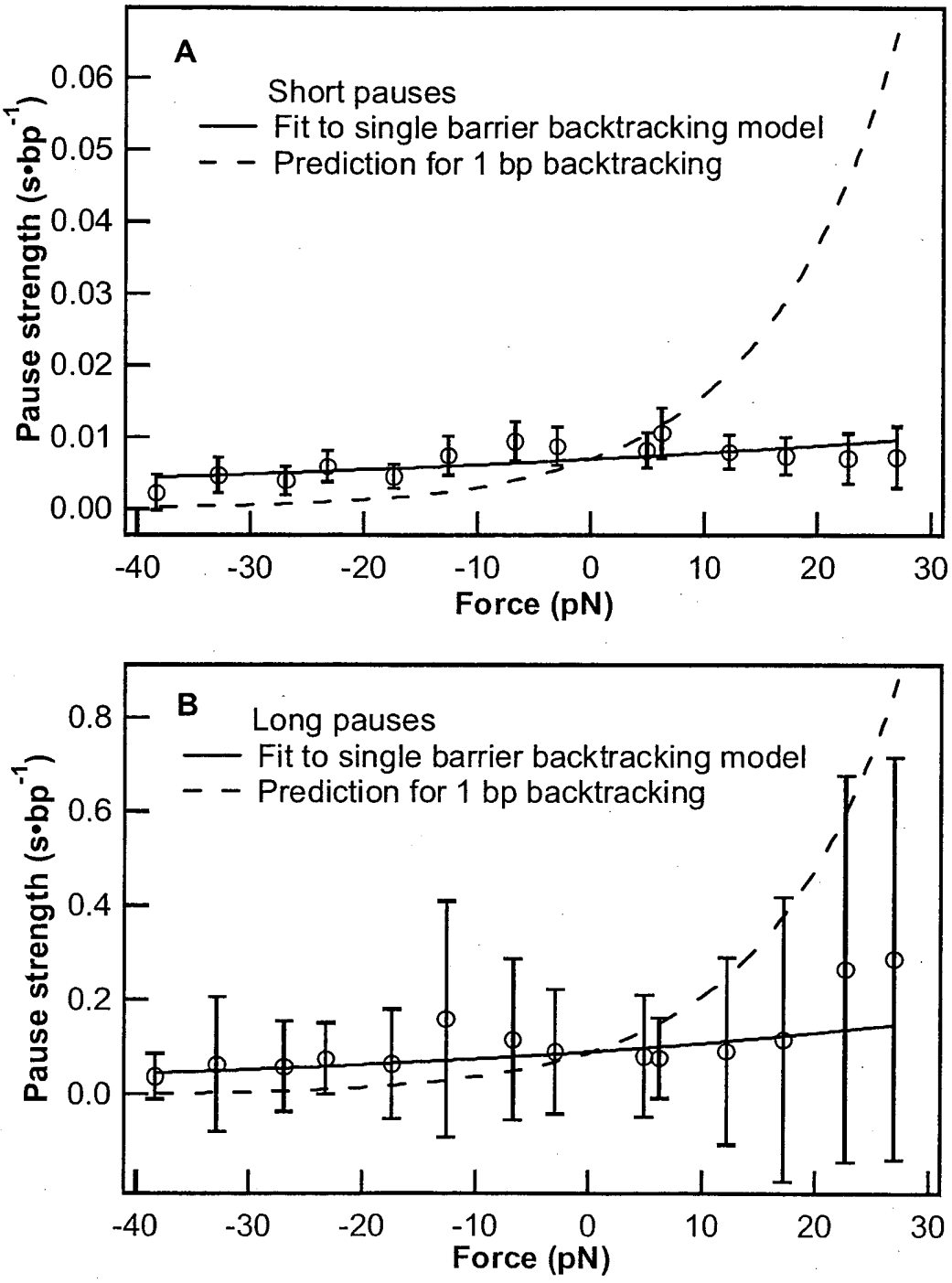

Figure 3.7. Pause strength as a function of load for short and long pauses. Pause strength is the product of pause duration and pause density. Pause strength was calculated from

the data in Fig. 3.6B and is plotted against the force (mean ± s.d.) along with the expected curve for a 1 bp backtracking displacement associated with pausing (δ_{total} = 1bp). A. Pause strength for short pauses. Fit to single barrier backtracking model (blue line) gives a $\delta_{total} = 0.14 \pm 0.07$ bp. B. Pause strength for long pauses. Fit to single barrier backtracking model (red line) gives a $\delta_{total} = 0.2 \pm 0.2$ bp.

different origin. The lack of significant sequence dependence of pause probability (Fig. 3.5) or pause duration (data not shown), make a direct search for pause sequences difficult. The question can be addressed from the opposite direction by computing the density of nucleotides and dinucleotides thought to promote pausing (Aivazashvili et al., 1981a; Aivazashvili et al., 1981b). A comparison between the density of the nucleotide uracil, or the dinucleotide pairs: uracil-guanine, uracil-purine, and pyrimidine-purine, thought to promote pausing, and the measured pause density (Fig 3.5) shows no strong correlation (data not shown). The origin of the transient pauses remains unclear. Further experiments with improved absolute position resolution or with defined templates will aid in elucidating the mechanism of transient pausing.

In the absence of motion associated with transient pauses, the conclusions from the F-V relationship must be revisited. The large displacement associated with the decrease of velocity and stall at high loads is at variance with the results from the transient pauses and suggests that the two processes arise from different mechanisms. Rather than simply increasing the probability and duration of naturally occurring pauses, the application of load appears to induce stalling through a distinct pathway. Pausing or stalling via this pathway is associated with a many bp transition, which may correspond to a displacement along the DNA template akin to backtracking or possibly a reorganization with the RNAP molecule itself. The model describing the F-V relationship (Equation 3.1) describes a class of models in which force dependent, off pathway, staling is one possible description. Other models that generate the same F-V relationship postulate a load dependent step in the translocation cycle (Wang et al., 1998). While any of these models

is formally possible, we favor the load-dependent stalling model, as it is observed that molecules do not immediately recommence translocation following a force-induced stall and some become irreversibly stalled (data not shown and Wang et al., 1998). This favors a scenario in which some reorganization or displacement must take place before the stall can be relieved.

Conclusion

Improvements in the optical trapping instrument and the single molecule transcription assay have permitted the acquisition of high-resolution recordings of single RNAP molecules transcribing under both assisting and hindering loads. Analysis of these records has lead to several results. Transient pausing with at least two lifetimes is ubiquitous within the gene studied. These pauses do not result from backtracking as evidenced by their insensitivity to applied load. In contrast, the F-V relationship indicates a large distance associated with force-dependent stalling. We propose that transient pausing and force-induced pausing represent two paused states with different origins. Extension of the F-V curve into the regime of assisting loads confirms that translocation is not the rate-determining step in transcription (Wang et al., 1998). Analysis of the velocity distribution of single molecules and their ensemble distribution suggest that there are multiple, widely distributed, velocity states, but that individual molecules do not switch between these states on measurable timescales. This contradicts the finding that RNAP molecules switch between two distinct velocity states (Davenport et al., 2000). Limited spatial and temporal resolution of that experiment could account

for the discrepancy (Guthold and Erie, 2001). The ability to distinguish short pauses from transcription allows the interplay between pausing and velocity to be investigated. Our results suggest that neither the discrepancy between transcription rates measured *in vivo* and *in vitro*, nor the variance in the population velocity distribution can be explained by the observed pauses.

The results and the conclusions drawn from them serve to raise as many questions as they have addressed. Foremost among these questions is the origin of the transient pauses. The limited absolute spatial resolution of single molecule techniques makes this a difficult question to address. As resolution and stability increases these experiments will provide more useful information. In the meantime, the ability to observe single molecules of RNAP transcribing over thousands of nucleotides with very high temporal resolution provides a unique tool with which to study transcription.

Materials and Methods

DNA template

Transcription experiments employed DNA templates generated by 28 PCR cycles with an XL PCR kit (Applied Biosystems) from plasmid pRL732, which was constructed by

inserting the region between BstXI and BstEII from plasmid pRL574 (Schafer et al., 1991) into the same sites in pRL777. pRL777 was produced by inserting the SacI-SpeI region of pCL102B (Chan and Landick, 1997) into the SacI-XbaI sites of pRL651 (Yin et al., 1999). The transcription template contains 1098 bp of DNA upstream of the T7 A1 promoter, which was followed by 3792 bp of the *E. coli rpoB* gene. For assisting force experiments the upstream primer was 5' digoxigenin labeled (all primers from Operon.), whereas for hindering force experiments the downstream primer was digoxigenin labeled.

Avidin coated beads

500 nm diameter carboxy-modified latex beads (Bangs Laboratories.) were covalently biotinated with biotin-x-caderverine (Molecular Probes), coated with avidin-DN (Vector Laboratories) and purified by repeated pelleting and re-suspension followed by sonication to eliminate clumping. Bead concentration was determined by absorption measurements made at 500 nm and compared with a standard curve.

Stalled RNAP ternary complexes

Assembly and purification of stalled ternary complexes has been previously described (Yin et al., 1994). Complexes stalled at A29 were obtained by incubating purified, biotin-labeled *E. coli* RNAP with DNA template, ATP, GTP and CTP (Roche Molecular Biochemicals) supplemented with [α-P^{32}]-GTP (Amersham Pharmacia Biotech). The stalled complexes were purified on a gel-filtration column and were quantified by scintillation counting. Beads were attached to the biotin label on the RNAP by

incubating 3-fold excess avidin-coated beads with the stalled complexes, which ensures that less than 5% of the beads will have multiple complexes bound to them.

Flow cell preparation for trapping experiments

Flowcells were assembled from #1½ glass coverslips (Corning) attached to a microscope slide (Corning) with two strips of double-sticky tape, arranged so as to form a channel (~0.5 cm wide) running across the narrow axis of the slide. To reduce mechanical drift, the double-sticky tape was supplemented with UV cured, low-viscosity epoxy (Master Bond), which was flowed into the space outside of the channel between the coverglass and the slide. Prior to assembly, the coverslips were sonicated in a KOH-ethanol solution, rinsed with de-ionized water and dried in an oven. The slides were soaked in ethanol, rinsed with de-ionized water, and dried. Flow cells for optical tapping experiments were first incubated for 40 minutes with 20 μg/ml of anti-digoxigenin polyclonal antibody (Roche Molecular Biochemicals) dissolved in PBS and washed with transcription buffer (PHC buffer: 50 mM HEPES-OH, pH 8.0, 130 mM KCl, 4mM $MgCl_2$,0.1 mM EDTA, 0.1 mM DTT, 20μg/ml Heparin). Non-specific binding of beads was reduced by incubating the flow cells with 3mg/ml BSA (Calbiochem) in transcription buffer for 20 minutes, after which the flowcells were washed with transcription buffer and incubated with stalled transcription complexes for 15 minutes followed by a final wash. Flow cells were kept at 4° C until used. To reduce thermal drift each flow cell was equilibrated for ~ 30 minutes on the optical-trapping microscope before taking measurements. Stalled complexes were restarted by perfusing the flow cell with transcription buffer supplemented with 1 mM NTPs (Roche Molecular Biochemicals) and

an oxygen scavenger system consisting of glucose oxidase (Calbiochem) 50 units/ml, catalase (Calbiochem) 10 units/ml, and glucose (Sigma) 450 mg/ml, to prevent photodamage from the optical trap (Neuman et al., 1999).

Optical trap

The optical trap employed for these experiments has been previously described (Svoboda and Block, 1994b; Wang et al., 1997). The instrument was enhanced by adding a feedback equipped piezoelectric stage (Physik Instrumente), which affords three-dimensional positioning with an accuracy and precision on the order of one nm. The piezoelectric stage allowed for a 2-dimensional calibration (one dimension in the specimen plane and one in the orthogonal dimension, along the optical axis of the trap) of both position and force of a bead in the optical trap (manuscript in preparation; (Pralle et al., 1999a; Rohrbach and Stelzer, 2002a). In addition, the stage could be incorporated into a force-feedback loop (Brower-Toland et al., 2002), which permitted recording motion over many microns while maintaining a constant force.

Position and force calibration

Axial position detection based on forward scattered light has been described (Pralle et al., 1999b; Rohrbach and Stelzer, 2002a). We have combined this technique with interferometric position detection as previously described for our instrument (Svoboda and Block, 1994b; Wang et al., 1997). Details of the combined position detection will be presented elsewhere. Briefly, the 2-dimensional position calibration of the optical trap was determined by moving a bead affixed to the surface of a coverslip in a raster scan

pattern in x (in the trapping or specimen plane) and z (along the optical axis, perpendicular to the trapping plane) and recording the interferometric x position signal and the total scattered light which reflects the z position of the bead. The resulting surface was fit with a 7^{th} order, 2-dimensional polynomial relating the measured x and z signals to actual positions in the optical trap. Trap stiffness in x and z was measured by a combination of frequency roll-off, variance and drag force measurements (Svoboda and Block, 1994a). In addition, the small increase in lateral stiffness as the bead is pulled away from the equilibrium trapping position in z was determined. We estimate the absolute uncertainty in force to be ~%15, due to the combined uncertainties in position measurement and force calibration.

Optical trapping

The optical trap could be operated in three modes. The position-clamp mode, in which the bead is prevented from moving past a defined point in the trap by changing the stiffness, has been previously described (Wang et al., 1998; Wang et al., 1997). This mode is well-suited to measuring stall forces and force-velocity relationships for single enzymes. The force-clamp mode, in which the position of the bead in the optical trap is held constant by moving the trap or the enzyme support (Visscher and Block, 1998; Visscher et al., 1999), is well-suited for measuring motion over long distances. We developed a stage-based force feedback system in which the stage moves to compensate for the motion of the enzyme, thereby maintaining the bead at a fixed position in the optical trap (Brower-Toland et al., 2002). The third mode is a force ramp mode in which the position of the bead is held fixed in the trap by moving the stage while the stiffness is

changed over time. This mode was employed to record the single enzyme force-velocity curves in the assisting force regime.

Data collection

After restarting the stalled ternary RNAP complexes, the bead was captured in the optical trap. The surface of the flow cell was found by raising the coverslip until the bead was moved slightly out of the optical trap in the axial direction. As the bead moved through the trap, the intensity of the scattered light displayed a reproducible peak that was a fixed distance from the surface of the coverslip, permitting surface determination to within 10 nm (manuscript in preparation). Once this position was determined, the stage was lowered such that the trap was centered 300 nm above the surface. Motion of the stage was corrected for the mismatch between the indices of refraction at the coverslip-sample interface that result in a scaling factor of 0.80 between the physical motion of the stage and the change in the trap center position (Wiersma et al., 1998). After setting the vertical position of the bead, the stage was moved back and forth, to generate a DNA stretching curve (Wang et al., 1997), which was used to determine the tether attachment point (Wang et al., 1997). The stage was then moved to center the trap on the tether attachment point at which point data collection began. The process of finding the surface and centering the tether point was largely automated which reduced the time between NTP addition and the start of recording to ~1 min. During an experimental run, the x and z position signals were low-pass filtered at 1 kHz, digitized at 2 kHz by means of a National Instruments DAQ board and boxcar averaged over 40 points to generate a 50 Hz signal that controlled the motion of the stage. Software for running the optical trap and

data acquisition was written in Labview (National Instruments). Motion of the stage and total laser intensity, which is linearly related to the trap stiffness, were recorded to hard disk for off-line analysis.

Data reduction

Motion of the stage was corrected for the elastic compliance of the DNA (Bouchiat et al., 1999; Marko and Siggia, 1995; Wang et al., 1997) and the displacement of the bead from the trap center to recover the contour length of the DNA as a function of time. Motion of the RNAP along the template was determined by subtracting the initial tether length from the computed DNA contour length and converting into bp by assuming 0.338 nm per bp. Precision of the position measurement was limited largely by the Brownian noise associated with the bead, which was governed by the combined stiffness of the trap and the DNA tether. Uncertainty in position measured at 50 Hz varied from 10 bp at 5 pN to 2 bp at forces > 35 pN. Absolute accuracy of the measurements was limited by stage drift. The average drift rate of 0.6 bp/s was low compared with the average transcription rate of ~10 bp/s. Over the duration of a long run, however, the accumulated error could be quite large, on the order of 200 bp. There was also an absolute position uncertainty associated with the initial centering of the tether and the dispersion in the bead size (~2%), which was estimated as 45 bp. Thus, the motion of the bead was well resolved in these experiments, but the absolute position of the RNAP along the template had a large uncertainty. In principle, individual traces can be corrected for the measured drift and the physical constraints of known tether length can be applied to correct the initial offset errors. Additionally, for traces that contain reproducible features, correlation techniques

would allow traces to be aligned with one another, if not absolutely. These procedures, however, have associated errors and uncertainties. For the data presented these corrections did not significantly change the conclusions based on absolute position information (see Fig. 3.5). For this reason the data are presented without these corrections.

The time dependent position of the RNAP molecule along the template was smoothed with a 2^{nd} order Savitzky-Golay filter with a time constant of 2.5 s and differentiated to generate the instantaneous velocity (Fig.3.2). The velocity distribution was fit with the sum of two Gaussians (Fig. 3.2 and Fig. 3.3A). Invariably there was a narrow peak near zero bp/s and a much broader peak centered at a positive velocity. The average transcription rate was calculated as the difference between the two peaks of the fitted curves (Fig. 3.3B). Pauses were scored when the velocity fell below half the Gaussian peak velocity. The results were largely independent of the exact choice of threshold pause velocity. Using a threshold velocity of one or two standard deviations from the pause or velocity peak changed the pause statistics slightly but did not change the overall conclusions. Data reduction and analysis were performed with custom software programmed in Igor Pro (Wavemetrics).

Simulations

Monte-Carlo simulations of transcription and transcriptional pausing were run to test the efficiency and accuracy of the pause detection algorithm and to optimize pause detection parameters. The simulated traces consisted of pauses of known duration and position interrupting periods of constant or stochastic motion or completely stochastic motion

defined by an average rate, pause probabilities, and durations and a number of rate limiting steps of equal duration. Stochastic pausing simulations were based on the assumption of an off-pathway pause state. Decisions with respect to filter type, order and time constant, as well as the velocity threshold, were based on these simulations. Parameters were chosen to allow the detection of pauses as short as one second with greater than 95% efficiency while limiting false pauses to a minimum. We were also able to quantify the effects of the pause detection algorithm on the underlying pause distribution. A slight deviation between measured and actual pause lifetime distribution was observed at a lifetime of 1.5 seconds and shorter. The reported uncertainties in the lifetime measurements reflect this artifact. Simulations were written and analyzed in Igor Pro (Wavemetrics).

References

Aivazashvili, V. A., Bibilashvili, R., Vartikian, R. M., and Kutateladze, T. A. (1981a). [Effect of the primary structure of RNA on the pulse character of RNA elongation in vitro by Escherichia coli RNA polymerase: a model]. Mol Biol (Mosk) *15*, 915-929.

Aivazashvili, V. A., Bibilashvili, R., Vartikian, R. M., and Kutateladze, T. V. (1981b). [Factors influencing the pulse character of RNA elongation in vitro by E. coli RNA polymerase]. Mol Biol (Mosk) *15*, 653-667.

Artsimovitch, I., and Landick, R. (1998). Interaction of a nascent RNA structure with RNA polymerase is required for hairpin-dependent transcriptional pausing but not for transcript release. Genes Dev *12*, 3110-3122.

Artsimovitch, I., and Landick, R. (2000). Pausing by bacterial RNA polymerase is mediated by mechanistically distinct classes of signals. Proc Natl Acad Sci U S A *97*, 7090-7095.

Bouchiat, C., Wang, M. D., Allemand, J., Strick, T., Block, S. M., and Croquette, V. (1999). Estimating the persistence length of a worm-like chain molecule from force-extension measurements. Biophys J *76*, 409-413.

Brower-Toland, B. D., Smith, C. L., Yeh, R. C., Lis, J. T., Peterson, C. L., and Wang, M. D. (2002). Mechanical disruption of individual nucleosomes reveals a reversible multistage release of DNA. Proc Natl Acad Sci U S A *99*, 1960-1965.

Chan, C. L., and Landick, R. (1989). The Salmonella typhimurium his operon leader region contains an RNA hairpin-dependent transcription pause site. Mechanistic implications of the effect on pausing of altered RNA hairpins. J Biol Chem *264*, 20796-20804.

Chan, C. L., and Landick, R. (1994). New perspectives on RNA chain elongation and termination by *E. coli* RNA polymerase. In Transcription: Mechanisms and Regulation, R. C. Conaway, and J. W. Conaway, eds. (New York, Raven Press), pp. 297-322.

Chan, C. L., and Landick, R. (1997). Effects of neutral salts on RNA chain elongation and pausing by Escherichia coli RNA polymerase. J Mol Biol *268*, 37-53.

Davenport, R. J., Wuite, G. J., Landick, R., and Bustamante, C. (2000). Single-molecule study of transcriptional pausing and arrest by E. coli RNA polymerase. Science *287*, 2497-2500.

Gittes, F., and Schmidt, C. F. (1998). Interference model for back-focal-plane displacement detection in optical tweezers. Optics Letters *23*, 7-9.

Guthold, M., and Erie, D. A. (2001). Single-molecule study reveals a complex E. coli RNA polymerase. Chembiochem *2*, 167-170.

Kassavetis, G. A., and Chamberlin, M. J. (1981). Pausing and termination of transcription within the early region of bacteriophage T7 DNA in vitro. J Biol Chem *256*, 2777-2786.
Komissarova, N., and Kashlev, M. (1997a). RNA polymerase switches between inactivated and activated states By translocating back and forth along the DNA and the RNA. J Biol Chem *272*, 15329-15338.

Komissarova, N., and Kashlev, M. (1997b). Transcriptional arrest: Escherichia coli RNA polymerase translocates backward, leaving the 3' end of the RNA intact and extruded. Proc Natl Acad Sci U S A *94*, 1755-1760.

Landick, R. (1997). RNA polymerase slides home: pause and termination site recognition. Cell *88*, 741-744.

Landick, R., Carey, J., and Yanofsky, C. (1987). Detection of transcription-pausing in vivo in the trp operon leader region. Proc Natl Acad Sci U S A *84*, 1507-1511.

Landick, R., Wang, D., and Chan, C. L. (1996). Quantitative analysis of transcriptional pausing by Escherichia coli RNA polymerase: his leader pause site as paradigm. Methods Enzymol *274*, 334-353.

Landick, R., and Yanofsky, C. (1987). Transcription attenuation. In *Escherichia coli* and *Salmonella*: Cellular and Molecular Biology, F. C. Neidhardt, ed. (Washington, DC, American Society for Microbiology), pp. 1276-1301.

Levin, J. R., and Chamberlin, M. J. (1987). Mapping and characterization of transcriptional pause sites in the early genetic region of bacteriophage T7. J Mol Biol *196*, 61-84.

Lyakhov, D. L., He, B., Zhang, X., Studier, F. W., Dunn, J. J., and McAllister, W. T. (1998). Pausing and termination by bacteriophage T7 RNA polymerase. J Mol Biol *280*, 201-213.

Marko, J. F., and Siggia, E. D. (1995). Stretching D. N. A. In Macromolecules, pp. 8759 (8712 pages).

Matsuzaki, H., Kassavetis, G. A., and Geiduschek, E. P. (1994). Analysis of RNA chain elongation and termination by Saccharomyces cerevisiae RNA polymerase III. J Mol Biol *235*, 1173-1192.

Mehta, A. D., Pullen, K. A., and Spudich, J. A. (1998). Single molecule biochemistry using optical tweezers. Febs Letters *430*, 23-27.

Mehta, A. D., Rief, M., Spudich, J. A., Smith, D. A., and Simmons, R. M. (1999). Single-molecule biomechanics with optical methods. Science *283*, 1689-1695.

Moerner, W. E., and Orrit, M. (1999). Illuminating single molecules in condensed matter. Science *283*, 1670-1676.

Mooney, R. A., Artsimovitch, I., and Landick, R. (1998). Information processing by RNA polymerase: recognition of regulatory signals during RNA chain elongation. J Bacteriol *180*, 3265-3275.

Neuman, K. C., Chadd, E. H., Liou, G. F., Bergman, K., and Block, S. M. (1999). Characterization of photodamage to escherichia coli in optical traps. Biophys J *77*, 2856-2863.

Nudler, E. (1999). Transcription elongation: structural basis and mechanisms. J Mol Biol *288*, 1-12.

Nudler, E., Mustaev, A., Lukhtanov, E., and Goldfarb, A. (1997). The RNA-DNA hybrid maintains the register of transcription by preventing backtracking of RNA polymerase. Cell *89*, 33-41.

Palangat, M., and Landick, R. (2001). Roles of RNA:DNA hybrid stability, RNA structure, and active site conformation in pausing by human RNA polymerase II. J Mol Biol *311*, 265-282.

Pralle, A., Prummer, M., Florin, E. L., Stelzer, E. H., and Horber, J. K. (1999a). Three-dimensional high-resolution particle tracking for optical tweezers by forward scattered light. Microsc Res Tech *44*, 378-386.

Reeder, T. C., and Hawley, D. K. (1996). Promoter proximal sequences modulate RNA polymerase II elongation by a novel mechanism. Cell *87*, 767-777.

Reisbig, R. R., and Hearst, J. E. (1981). Escherichia coli deoxyribonucleic acid dependent ribonucleic acid polymerase transcriptional pause sites on SV40 DNA F1. Biochemistry *20*, 1907-1918.

Richardson, J. P., and Greenblatt, J. (1996). Control of RNA chain elongation and termination. In *Escherichia coli* and *Salmonella*: Cellular and Molecular Biology, F. C. Neidhardt, ed. (Washington, DC, American Society for Microbiology), pp. 822-848.

Rohrbach, A., and Stelzer, E. (2002a). Three-dimensional position detection of optically trapped dielectric particles. JOURNAL OF APPLIED PHYSICS *91 (8):*, 5474-5488.

Schafer, D. A., Gelles, J., Sheetz, M. P., and Landick, R. (1991). Transcription by single molecules of RNA polymerase observed by light microscopy. Nature *352*, 444-448.

Stelzer, E. H. K., Florin, E. L., Pralle, A., and Horber, J. K. H. (1998). Photonic force microscope based on optical tweezers and two-photon excitation for biological applications. Abstracts of Papers of the American Chemical Society *216(pt.1)*, 336-COLL.

Svoboda, K., and Block, S. M. (1994a). Biological applications of optical forces. Annu Rev Biophys Biomol Struct *23*, 247-285.

Svoboda, K., and Block, S. M. (1994b). Force and velocity measured for single kinesin molecules. Cell *77*, 773-784.

Toulme, F., Guerin, M., Robichon, N., Leng, M., and Rahmouni, A. R. (1999). In vivo evidence for back and forth oscillations of the transcription elongation complex. Embo J *18*, 5052-5060.

Uptain, S. M., and Chamberlin, M. J. (1997). Escherichia coli RNA polymerase terminates transcription efficiently at rho-independent terminators on single-stranded DNA templates. Proc Natl Acad Sci U S A *94*, 13548-13553.

Uptain, S. M., Kane, C. M., and Chamberlin, M. J. (1997). Basic mechanisms of transcript elongation and its regulation. Annu Rev Biochem *66*, 117-172.

Visscher, K., and Block, S. M. (1998). Versatile optical traps with feedback control. Methods Enzymol *298*, 460-489.

Visscher, K., Gross, S. P., and Block, S. M. (1996). Construction of multiple-beam optical traps with nanometer-resolution position sensing. IEEE Journal of Selected Topics in Quantum Electronics *2*, 1066-1076.

Visscher, K., Schnitzer, M. J., and Block, S. M. (1999). Single kinesin molecules studied with a molecular force clamp. Nature *400*, 184-189.

Wang, M. D., Schnitzer, M. J., Yin, H., Landick, R., Gelles, J., and Block, S. M. (1998). Force and velocity measured for single molecules of RNA polymerase. Science *282*, 902-907.

Wang, M. D., Yin, H., Landick, R., Gelles, J., and Block, S. M. (1997). Stretching DNA with optical tweezers. Biophys J *72*, 1335-1346.

Weiss, S. (1999). Fluorescence Spectroscopy of Single Biomolecules. Science *283*, 1676-1695.

Wiersma, S. H., Torok, P., Visser, T. D., and Varga, P. (1997). Comparison of different theories for focusing through a plane interface. Journal of the Optical Society of America a-Optics Image Science and Vision *14*, 1482-1490.

Yin, H., Artsimovitch, I., Landick, R., and Gelles, J. (1999). Nonequilibrium mechanism of transcription termination from observations of single RNA polymerase molecules. Proc Natl Acad Sci U S A *96*, 13124-13129.

Yin, H., Landick, R., and Gelles, J. (1994). Tethered particle motion method for studying transcript elongation by a single RNA polymerase molecule. Biophys J *67*, 2468-2478.

Yin, H., Wang, M. D., Svoboda, K., Landick, R., Block, S. M., and Gelles, J. (1995). Transcription against an applied force. Science *270*, 1653-1657.

Conclusion and future directions

We have presented a series of experiments that culminated in the ultimate goal of measuring transcription by single molecules of RNA polymerase. Some of the results obtained during this process are more generally applicable and have suggested further experiments.

We measured a complex wavelength dependence of optical damage of trapped *E. coli*, and we determined that this does not originate from simple heating effects. The similarity of the damage spectrum for *E. coli* and for mammalian cells determined by another lab (Liang, H., Vu, K. T., Krishnan, P., Trang, T. C., Shin, D., Kimel, S., and Berns, M. W. (1996). Wavelength dependence of cell cloning efficiency after optical trapping. Biophys J *70*, 1529-1533), suggests that these results are of general applicability and implicate an unknown but ubiquitous molecule as the causative agent of photodamage. Furthermore, we established that photodamage could be eliminated by removing the molecular oxygen in the trapping medium. Whereas this work provided a solution to optical damage, it failed to determine the precise origin of the damage. This question can be addressed through several different experiments. The role of singlet oxygen or other free radicals can be tested through the effects of scavenger molecules that will specifically neutralize different radical species. To test for the involvement of singlet oxygen specifically, cells can be trapped in Deuterium oxide, in which the lifetime of singlet oxygen is an order of magnitude longer than in water. As singlet oxygen is the most likely candidate for the causative agent of photodamage, trapping with a laser with a

wavelength longer than the lowest excitation of molecular oxygen may eliminate photodamage.

In the next phase of the project, we extended the detection capabilities of the optical trap to include the axial dimension. In this work, we improved on a previously described technique of axial detection, and we developed novel techniques of determining the absolute axial position of trapped particle. These techniques allowed us to make an important correction to the force on a trapped particle that is displaced in the axial direction. Whereas the majority of this work involved the development of techniques and improved measurement capabilities, it also allowed us to accurately measure the focal shift that occurs on focusing through an interface between mismatched indices of refraction. This is an important consideration in high-resolution confocal and fluorescent microscopy and has been a subject of theoretical investigation. Preliminary calculations do not agree with the measured focal shift. We are currently undertaking a more thorough investigation of the focal shift problem both experimentally and theoretically. The culmination of these experiments was the single-molecule study of RNAP with the improved optical tweezers instrument. In this study we identified a class of transient pauses on a template that was devoid of known regulatory pauses. The duration and probability of these pauses remained independent of load over a 70 pN range. This finding challenges a proposed model of transcription in which such transient pauses are associated with backtracking of the enzyme along the DNA template. Measurements of transcription velocity revealed that individual enzymes move with a single velocity or a narrow spread of velocities but that this velocity is chosen from a wide distribution of

velocity states. Extension of the force velocity relationship of RNAP into the regime of assisting loads, which did not increase the velocity, verified that the translocation step in the enzymatic cycle of RNAP is not rate determining at low loads. As has been the case with much of the work on RNAP, this work served to raise more questions that it served to address. This work will be continued in a series of experiments at Stanford. One of the few drawbacks of the optical trapping experiment was the lack absolute positional information on the base pair level. This prevented a thorough comparison of the motion and pauses with the sequence or from trace to trace. This is being addressed on two fronts. The stability and long-term drift of the instrument and the assay are being improved. We have also developed a template that has specific long-duration regulatory pauses at defined points. These pauses will not only serve as fiducial points in the traces but are an interesting candidate of study themselves. One such template includes a pause sequence that induces backtracking, which will allow us to directly test the effect of force on the backtracked state. Another approach to the problem of absolute positional uncertainty is to use a homogenous template. RNAP will not transcribe a homo-polymer DNA sequence but it will transcribe an alternating co-polymer. Studying transcription on such a template provides many possibilities. The velocity, pausing and maximum force can be studied for different enzymes in the absence of DNA sequence effects. Furthermore, the limited number of nucleotides required for transcription of such a template will allow very precise measurements of kinetic parameters such as incorporation rates and competitive inhibition by other nucleotides. Potentially the most interesting aspect of the co-polymer templates would be the ability to eliminate secondary structure in the nascent RNA. Secondary structure has been tied to both pausing and to

the stability of the transcribing complex. Investigating transcription in the absence of secondary structure will shed light on its role in transcription. In a related experiment, we plan on applying load on the RNA transcript rather than the enzyme directly. This will provide a measure of the stability of the transcribing complex, and at loads sufficient to unfold nascent RNA structure, will provide a means of studying transcription in the absence of secondary structure. These experiments highlight the power of optical trapping in the study of this and other processive motor enzymes. The potential of this technique is just now being realized and should provide a wealth of new insights in the near future.